

Chapter 9

Impurity Defects in Diamond

In the following seven sections, the spectral lines (and bands) from impurity defects are described.

Six important impurities are nitrogen (Sect. 9.1), boron (Sect. 9.2), hydrogen (Sect. 9.3), silicon (Sect. 9.4), nickel (Sect. 9.5), and cobalt (Sect. 9.6).

In Sect. 9.7, lines from 18 other impurities are listed, and a general discussion of impurity centers is given.

9.1 Nitrogen in Diamond

Nitrogen is the most common and also a very important impurity in natural and synthetic diamond (see the fundamental defects in Tables 1.1.1–1.1.2). Five of the six well-known infrared centers contain nitrogen (A–C, E, and F). The historical classification scheme for natural diamonds is based on the nitrogen content, i.e., type I for high and type II for low (< 40 ppm) nitrogen concentration, as monitored by the visible light absorption in the 2.5–5.5 eV range (see Sect. 1.2.1 [Rob34]).

There are five types (1–5) of the 42 nitrogen centers in diamond. The majority (30 centers, 2–4) are associates with intrinsic defects (see Chap. 8). The properties of the associates are dominantly determined by the intrinsic defects.

1. Nitrogen only (4): isolated substitutional nitrogen

$N_1^\circ = \mathbf{C}$ center (see Table 9.1.1.1)

$N_1^+ = \mathbf{E}$ or \mathbf{X} center (see Table 9.1.1.2)

$N_2 = \mathbf{A}$ center (see Table 9.1.1.3)

N_2^+ (see Table 9.1.1.3)

2. Associates (18) with lattice vacancies (see Tables 8.1.3.1–8.1.5):

($NV = V_1N_1^\circ$, $\mathbf{H2} = V_1N_2^-$, $\mathbf{H3} = V_1N_2^\circ$, $\mathbf{N3} = V_1N_3^\circ$, $\mathbf{N9} = V_1N_4^-$, $\mathbf{B} = V_1N_4^\circ$ (see Table 8.1.3.5), $\mathbf{F} = V_1N_4(C_2)_i^\circ$ (see Table 8.1.3.6), $\mathbf{H4} = V_2N_4^\circ$, etc.

3. Associates (6) of N_1 or N_2 with the $\langle 1\ 0\ 0 \rangle$ split carbon self-interstitial: ($5R_L = (C_2)_i N_1$, etc.) (see Table 8.2.3).
4. The $\langle 1\ 0\ 0 \rangle$ split $(N_1 C_1)_i$ *interstitial* (4) in three charge states: (**R11**, etc.), and related centers, like $(N_2)_i$ (see Table 8.2.4).
5. Donor–acceptor pairs (DAP) (9) of nitrogen with boron, and of nitrogen with an unknown acceptor (see Table 9.1.5).

9.1.1 Isolated Nitrogen Centers

$N_1^\circ = C$ center: The absorption lines and bands of the C center are listed in Table 9.1.1.1. In EPR, the paramagnetic N_1° center is known as the P1 center [New01a].

The properties of the single substitutional nitrogen (C center) have been the subject of numerous experimental and theoretical investigations. The C center is the dominant nitrogen center in type Ib diamonds. Type Ib is the common type in synthetic HPHT diamonds, but is seldom found among natural diamonds.

The original T_d symmetry is lowered to C_{3v} with a large gain in Jahn–Teller energy, and a considerable lowering of the donor level to a calculated position at 2.20 eV above the valence band, i.e., 3.30 eV below the conduction band [Mes73]. One of the four N–C bonds is elongated by ca. 26%, where the two atoms move apart by roughly the same amount [Mes73, Mai94a].

With partial ^{13}C substitution (40%, 50%, 70%, 95% ^{13}C), a splitting into four to five lines of the 167-meV line (100%C, 0%N) is observed [Col93e],[San93]. In the analysis by the present author, the vibration is located with 24% at C' (distorted direct neighbor of N), $1 \times 20\% + 2 \times 12\% = 44\%$ at $3 C''$ (three ligands of C' , further distorted), and $9 \times 3.5\% = 32\%$ at C''' (Nine ligands of $3 C''$). With these parameters (and a slight adjustment of the partial ^{13}C content, i.e., 44%, 56%, 75%, and 89%), the line shifts can be reproduced within 1% of the total shift (–52 meV). This fit is much better than that obtained previously with the force constant model [San93].

For the C center, three broad vibronic absorption bands are observed: $C(\alpha_2)$ at 3.30 eV, $C(\beta_2)$ at 3.90 eV, and $C(\gamma_2)$ at 4.55 eV. However, only for $C(\gamma_2)$ the corresponding ZPL is observed ($C(c)$ at 4.059 eV), with quasi-local vibrational mode (QLVM) sidebands at 4.120 and 4.179 eV. The two other ZPLs are expected at the onset of the absorption and luminescence bands: $*C(a)$ at 2.80 and $*C(b)$ at 3.40 eV (see Table 9.1.1.1).

The DAP1 analysis (see Table 10.3) yields for the N_1° donor ground level a position at 3.23 eV below the conduction band (close to the theoretical value of 3.30 eV [Mes73], see below). Therefore, the excited state of $*C(a)$ would be in the energy gap, while the excited states of $*C(b)$ and $C(c)$ would be inside the conduction band. This interpretation is in agreement with the (very weak) photocurrent (PC) at 3.30–4.05 eV, with the PC peak = $C(\beta_2)$ at 3.90 eV, and the intense PC starting at 4.05 eV with the (not resolved) PC peak $C(\gamma_2)$ at 4.55 eV [Den67]. Structure on this band with onset at 4.070, 4.150, and 4.240 eV

Table 9.1.1.1 Transitions from the neutral isolated substitutional nitrogen atom in diamond ($N_1^0 = C$ center; in EPR: P1 center)

Line/ band ^a	E (meV) (cm^{-1})	Width (meV) (%)	Relat. int. (%)	i13 shift ^b $^{13}E/$ $^{12}E(\%)$	i15 shift ^c $^{15}E\perp$ $^{14}E(\%)$	Comment, percentage of C or N vibrational involvement from isotope shifts
C(a')	105.4	25	36	–	–	N–C or C–C bend vibration
	850	24				
C(b')	129.6	7	7	–4.1	–	100%C
	1,045	5				
C(c')	136.0	3	1	–4.3	–	100%C
	1,097	2				
C(d')	140.1	8	28	–2.9	–1.3	70%C – 30%N vibration var. 138.7– 140.7 meV
	1,130	6				
C(e')	149.5	14	23	–3.9	–	100%C
	1,206	9				
C(f')	161.2	5	4	–4.4	± 0	100%C
	1,300	3				
C(g')	166.6	0.6	1	–3.9	± 0	100%C (see also text Sect. 9.1.1)
	1,344	0.4				
	E (eV)	Width (eV)				
*C(α 1)	2.30	0.40	–	–	–	Luminescence band
(*C(a))	(2.80)	–	–	–	–	Expected ZPL (onset of C(α 1) and C(α 2))
C(α 2)	3.30	0.60	–	–	–	Polarized absorption band, E //trigonal axis
*C(β 1)	2.88	0.35	–	–	–	Luminescence band
(*C(b))	(3.40)	–	–	–	–	Expected ZPL (onset of C(β 1) and C(β 2))
*C(β 2)	3.90	0.80	–	–	–	Polarized absorption band, E /trigonal axis

(continued)

Table 9.1.1.1 (continued)

Line/ band ^a	E (meV) (cm^{-1})	Width (meV) (%)	Relat. int. (%)	i13 shift ^b ¹³ E / ¹² E (%)	i15 shift ^c ¹⁵ E / ¹⁴ E (%)	Comment, percentage of C or N vibrational involvement from isotope shifts
C(c)	4.059	0.01	–	–	–	ZPL of C(γ); QLVM: +61 meV [Naz87]
*C(γ 2)	4.550	0.6	–	–	–	Polarized absorption band, E //trigonal axis

^aThe C(a'–g') IR and C(c) UV absorption lines are observed in NA, HA, and LA. The C(α 1)–C(γ 2) bands are observed in NB, HB, and LB. The C(c) line and the C(γ 2) band are also observed in photoconductivity (PC)

^bFrom [Col88c], Table 1 and Fig. 1;

^cFrom [Col82], [Dav94a]

corresponds to the ZPL = C(c) at 4.059, with two QLVM sidebands at 4.120 and 4.179 eV (see Table 9.1.1.1).

The depth of the isolated nitrogen donor has been the subject of several theoretical and experimental investigations (summarized in [Naz94a]).

In a pioneering theoretical treatment, a dramatic energy gain by a (1 1 1) Jahn–Teller distortion (26% lengthening of one N–C bond) was calculated [Mes73]. While the effective mass treatment predicts a depth of 0.4 eV for T_d symmetry, the depth for the C_{3v} distorted nitrogen in the cluster calculation is 3.3 eV (2.2 eV above the valence band).

From PC measurements, different depth values of **1.7 eV** (natural type Ib, [Far69], [Ver75]), **2.0 eV** (HPHT synthetic type Ib [Far74]), or **4.05 eV** (natural type Ia, Ib, or natural intermediate type [Den67, Dea65a]) have been derived.

However, a great difficulty in PC data interpretation arises from the fact that all transitions from standard DAP are expected to be PC active. Two clear examples of PC spectra with well-resolved features are (a) DAP32 = GR2–8 [Ver75b] and (b) DAP63/64 = N9 [Den67].

With the present knowledge, it can be concluded that none of the above-mentioned depth values (**1.7**, **2.0**, and **4.05 eV**) represents the true ionization energy of the $N_1^\circ = C$ center (which is **3.23 eV** from DAP1). Three possible explanations can be offered: (a) the onset at **1.7 eV** arises from DAP9 (E or X center + boron, 1.74–2.18 eV); (b) the onset at **2.0 eV** arises from DAP1 (C center + boron, 2.02–2.67 eV); and (c) the onset at **4.05 eV** arises from transitions from the ground state in the gap to excited states inside the conduction band (C center: 4.059 eV; B center: 4.184, 4.191, and 4.197 eV; and A center: 4.470 eV).

An isolated PC peak from a type Ia sample occurs at 4.7 eV [Den67] and can be assigned to the B(α 2) absorption peak at 4.7 eV. An unresolved PC peak at

Table 9.1.1.2 The positively charged isolated substitutional nitrogen atom in diamond: $N_1^+ = E$ (or X) center, IR absorption $E(a'-g')$, and PC bands $*E(\alpha 2 - \gamma 2)$

Line/ band $N_1^+E = X$	E (meV) (cm^{-1})	Width (meV)(%)	Relat. Int. (%)	i13 shift	i15 shift	Comment
$E(a')$	117.8	12	26	–	–	HA [Law93b]; Fig. 3.21
	950	24				MA [Col88c]; Fig. 3.15
$E(b')$	129.7	7	19	–	–	NA[Woo83]; Fig. 3.20,
	1,046	5				HA[Law93b]; Fig. 3.21 MA[Col88c]; Fig 3.15
$E(c')$	138.2	8	19	–	–	NA[Woo83]; Fig. 3.20,
	1,115	2				HA[Law93b]; Fig. 3.21, MA[Col88c]; Fig. 3.15
$*E(d')$	146.9	7	9	–	–	MA[Col88c]; Fig. 3.15
	1,185	6				Overlapping band
$*E(e')$	152.5	8	14	–	–	MA[Col88c]; Fig. 3.15
	1,230	9				Overlapping band
$*E(f')$	159.9	7	8	–	–	MA[Col88c]; Fig. 3.15
	1,290	3				Overlapping band
$E(g')$	165.1	0.7	5	–	–	HA[Law93b]; Fig. 3.21,
	1,332	0.4				MA[Col88c]; Fig. 3.15
	E (peak) (eV)	Width (eV)(%)				
$*E(\alpha 2)?$	2.50	0.30 12	–	–	–	From photoconductivity [Far74]
$*E(\beta 2)?$	3.50	0.45 13	–	–	–	From photoconductivity [Far74]
$*E(\gamma 2)?$	4.20	0.50 12	–	–	–	From photoconductivity [Far74]

Table 9.1.1.3 The neutral N_2° = A center (IR absorption and vibronic lines and bands), and the positively charged $*N_2^{+}$ center (vibronic lines)

Line/band	E (meV) (cm^{-1})	Width (meV) (%)	Relat. int. (%)	i15 shift $^{15}E/^{14}E$ E(%)	Comment
N_2°					
A(a')	60.0 <i>484</i>	6 <i>10</i>	11	–	N–C bond
A(b')	135.1 <i>1,090</i>	4 <i>3</i>	2	–	–
A(c')	146.9 <i>1,185</i>	7 <i>5</i>	21	–	–
A(d')	150.6 <i>1,215</i>	6 <i>4</i>	8	–	–
A(e')	158.9	7	58	–1.1 [Dav94b]	N(29%)–C(71%) stretch; close to the ZPL of SB-DAP30 from the $N_2 + V_1$ center: ($L =$ 0.154 , $D = 1.45$ eV) with lines H1 b, d, g
	<i>1,282</i> E (eV)	5 Width (eV)			
*A(a)	3.928	0.015	–	–	Named N6 , proposed LVM sideband at 4.088 eV (+160 meV = A(e'))
*A(α 2)	> 3.9	–	–	–	Absorption continuum with onset at 3.9 eV; photoconductivity threshold at 4.0 eV
*A(b)	4.470	0.010	–	–	ZPL; SB (QLVM) at $f = 58$, $w = 38$ meV [Naz87]; (calc. $f = 58.5$, $w = 36.3$ meV for N_1C_2 ; see Table 11.2)
*A(β 2)	5.00	0.60	–	–	Absorption (see Table 2.4.3) and PC [Den67] band
* N_2^{+} (a)?	1.602	0.012	–	–	Observed in PL; sidebands: QLVM at $f = -74$ meV, $w = 57$ meV (calc. $f =$ 74.5 , $w = 59$ meV for N_2 ; see Table 11.2); LVM (overlap) at -77 meV
* N_2^{+} (b)?	2.910	0.012	–	–	Observed in absorption and CL; LVM at -77 meV

5.00 eV from an intermediate type sample [Den67] corresponds probably to the $A(\beta_2)$ absorption peak at 5.00 eV.

$N_1^+ = E$ center or X lines: The assignment of the ($N_1^+ = E = X$) center was accomplished by a detailed study of the interconversion of N_1° and N_1^+ [Law98]. First, a synthetic HPHT diamond was irradiated with $2 \times 10^{18} \text{ cm}^{-2}$ 1.9-MeV electrons, which resulted in a ratio of 40% N_1° to 60% N_1^+ . Second, photochromic studies showed that a quantitative conversion from N_1^+ to N_1° occurs with UV illumination of $E > 3.1$ eV and the reverse process with illumination of $2.1 < E < 3.1$ eV [Law98].

The absorption lines and bands of the $E = X$ center are listed in Table 9.1.1.2. The IR spectrum of N_1^+ is similar to that of N_1° . Especially, the small shift in the sharp line from 166.6 (N_1°) to 165.1 meV (N_1^+) indicates similar distortions for both centers. The expected depth of N_1^+ is $E_D = 3.48$ eV (see DAP9, Table 9.1.5).

Also, the broad bands from N_1^+ transitions to the excited states (inside or near the conduction band) are similar to those of N_1° : $E(\alpha_2)/E(\beta_2)/E(\gamma_2) = 2.50/3.50/4.20$ eV, compared to that of $C(\alpha_2)/C(\beta_2)/C(\gamma_2) = 3.30/3.90/4.55$ eV.

$N_2^\circ = A$ center: The absorption lines and bands of the A center are listed in Table 9.1.3. The A center is paramagnetic in the ionized state.

From theory, it is known that the length of the N–N bond is increased by 30%, and the length of the N–C bond is decreased by 4% (compared to the lattice C–C bond) [Mai94a].

The DAP20 analysis (see Table 9.1.5) yields for the N_2° donor ground level a position at 3.71 eV below the conduction band. This is in good agreement with the observed onset of the absorption continuum at 3.9 eV. In the ultraviolet range, an absorption and PC band $A(\beta_2)$ at 5.00 eV with ZPL at 4.470 eV is observed (see Table 9.1.1.3).

*** N_2^+ center:** This center with a depth of 1.44 eV (see Table 9.1.5) is indirectly observed in the DAP67 ($*N_2^+ + B_1^\circ$) transitions (3.86–4.28 eV). A luminescence line at 1.602 eV in high nitrogen diamonds can possibly be assigned to $*N_2(a)$. In addition, a luminescence (2.897 eV) and absorption (2.910–2.916 eV) line can be tentatively assigned to $*N_2(b)$. This line appears in spectra of DAP18, e.g., in luminescence after N^+ implantation (and 1,400 °C anneal) of type IIa diamonds [Zai01]. Both ZPLs have a local vibrational mode (LVM) sideband at –77 meV (see Table 9.1.1.3).

9.1.2 Associates of Nitrogen with Single or Double Vacancies

$V_1N_1^-$; $V_1N_1^\circ$ (= NV center) and $V_1N_2^+$ (= S1 center): Details of these centers are given in Table 8.1.3.1. All three centers are observed in natural, as grown HPHT, or CVD synthetic diamonds, and also in irradiated (and annealed) diamond.

*** $(V_1H_1)^\circ N_1$:** This configuration is tentatively assigned to weak infrared lines from natural diamond (see Table 8.4a). The NH bend vibration is not directly observed, but can be indirectly determined from the stretch + bend combination line.

($V_1N_2^- = H2$ center) and ($V_1N_2^\circ = H3$ center): Details of these centers are given in Table 8.1.3.1. The **H2** center (1.256 eV, DAP77/78) appears after heating diamonds to 1,700 °C, or after irradiation and annealing at 500–1,500 °C. The **H3** center (2.464 eV, DAP51/52) is observed in natural, in HPHT or CVD synthetic, and in irradiated (and annealed) diamond. Photochromic interconversion of H2 and H3 is achieved by illumination below or above 600 nm (= 2.07 eV) [Mit90]. Uniaxial stress experiments on H2 [Law92b] and H3 [Dav76a, Dav76b] have shown that these centers have C_{2v} symmetry with the C_2 axis along (0 0 1) and two (1 1 0) reflection planes, i.e., the structure is N–V–N.

*** $V_1N_3^-(V_1N_3^\circ = N3$ center) and * $V_1N_3^\pm$:** Details of these centers are given in Table 8.1.3.2. The well-known N3 center has three ZPL transitions: $V_1N_3^\circ(a,b,c)$, at 2.297, 2.680, and 2.985 eV. There are luminescence sidebands (with structure) for $V_1N_3^\circ(a,b,c)$, but there is an absorption sideband (with structure) only for $V_1N_3^\circ(c)$. The transitions of $V_1N_3^\circ(a)$ and $V_1N_3^\circ(b)$ are observed only in delayed photoluminescence [Sob76].

*** $V_1N_3^\circ(C_2)_i$:** When the vacancy of the $V_1N_3^\circ$ center is created, a $(C_2)_i$ self-interstitial is expelled, which is later gathered in the platelets (see the discussion in Sect. 9.1.6.1). In an intermediate state (only with *small* platelets, 5 nm), the self-interstitial is connected to V_1N_3 , forming the * $V_1N_3^\circ(C_2)_i$ center (see Table 8.1.3.2). This center shows great similarity to $V_1N_3^\circ(a)$ (both centers observed only in delayed photoluminescence). The ZPL of $V_1N_3^\circ(C_2)_i$ is shifted by –95 meV with respect to the ZPL of the isolated $V_1N_3^\circ(a)$ (only with *large* platelets, 100 μm) [Sob76].

($V_1N_4^- = N9$ center) and ($V_1N_4^\circ = B$ center): For details of these centers, see Table 8.1.3.2. The ZPL absorption lines of the B center (in the ultraviolet) are very weak [Naz87]. The ZPL splitting of 6–7 meV is typical for a dynamic Jahn–Teller effect. Four lines of the sideband DAP82 are superimposed on the $B(\alpha)$ absorption band. The B center is well known for its vibrational infrared absorption lines (see Table 8.1.3.5).

The ZPL of the N9 center is split into three lines: N9(a) at 5.252, N9(b) at 5.262, and N9(c) at 5.277 eV. This 10–15 meV splitting is similar to that of the B center, indicating again a dynamic Jahn–Teller effect. Well-resolved lines from the sideband DAP63 (absorption) and the sideband DAP64 (luminescence) are observed.

*** $V_1N_4(C_2)_i^\circ = F$ center:** As described in Sect. 9.1.6.1, the self-interstitial is connected to ($V_1N_4^\circ = B$ center), forming the (* $V_1N_4(C_2)_i^\circ = F$ center). The ZPL of $V_1N_4(C_2)_i^\circ$ is shifted by +376 meV with respect to the ZPL of the isolated $V_1N_4^\circ(b)$. Similar to the B center, the F center has well-known vibrational infrared absorption lines, which correlate with the ZPL F(a) (see Table 8.1.3.3). However, compared to the vibrations of the B center (highest frequency 165 meV), the F center vibrations extend to 191 and 196 meV, which are typical frequencies of $(C_2)_i$ vibrations. There are three ZPL transitions at $F(a) = 2.145$, $F(b) = 2.721$, and $F(c) = 4.567$ eV, each with broad sidebands. The structure on the 5.0-eV sideband of F(c) reveals the involvement of donor–acceptor transitions (DAP81a–f).

$V_2N_1^\circ$, $V_2N_3^\circ$, and ($N_3V_2N_1^\circ = H4$ center): It has been shown by theory that the H4 center is formed when the ($V_1N_4 = B$ center) captures a vacancy

(see Eqs. (9.8a,b)). The infrared center with the lines $(H1(c, e, f) = V_1N_4^\circ + V_1^\circ)$ is an intermediate state (see the discussion below). A similar process can be assumed for the formation of V_2N_1 and V_2N_3 . Details of these centers are given in Table 8.1.3.4.

9.1.3 Associates of the Split Self-interstitial $(C_2)_i$ with One or Two Nitrogens

$*(C_2)_iN_1^\circ = 5RL$: The 5RL center (4.582 eV, DAP79/80) is prominent in as-irradiated diamonds, is enhanced by 500 °C anneal, and anneals out at 800–1,200 °C. The luminescence spectrum is unusual, showing four intense sidebands (partly exceeding the ZPL intensity) of the 237-meV C–C vibration. This gave rise to the name 5RL = “5 radiation lines.” The proposed structure is in good agreement with the observed vibrational frequencies and their isotope shifts [Col88c], and also with the uniaxial stress results [Col86b]. Details of the 5RL center are given in Table 8.2.3.

$*(C_2)_iN_1^+$: The positive charge state of the 5RL has properties similar to that of the neutral charge state (see Table 8.2.3).

$*(C_2)_iN_2^-$, $*(C_2)_iN_2^\circ$, $*(C_2)_iN_2^+$: The three charge states of the $*(C_2)_iN_2$ center have very similar properties (see Table 8.2.3).

9.1.4 The $\langle 100 \rangle$ Split Nitrogen–Carbon Interstitial $(N_1C_1)_i$ in Three Charge States, Associates with Boron, and the $(N_2)_i^\circ$ center

These seven centers are described in Sect. 8.2.4 and in Table 8.2.4.

9.1.5 Donor–Acceptor Pairs of Nitrogen (N_1 and N_2) with a Single Boron and of Nitrogen (N_2) with an Unknown Acceptor

$*N_1^\circ + B_1^\circ = DAP1$: For diamond, this is the first donor–acceptor pair system described in the literature [Dis94a,b]. The transitions of this standard DAP occur in the range 2.070–2.668 eV (shells $s = 50$ to $s = 1$). The DAP line of the nearest neighbor N–B pair ($s = 1$) is very intense, but no electronic transition from this center is observed. The notation is $*N_1^\circ + B_1$, which emphasizes the DAP character, and the $*$ indicates that the atomic composition is not yet fully confirmed.

Table 9.1.5 Donor–acceptor pairs (standard DAP) of a nitrogen donor (N_1 or N_2) with the boron acceptor

Defect	Observed L (eV)	Lines (range) (eV)	Standard-DAP	D (eV)	Name/comment	
$*N_1^\circ + B_1^-$	NL	1.871	1.559–1.791	106 a–k	–1.43	shells: 16, 20, 22, 24, 26, 32, 34, 54, 58, 198, 228/ $E_D + E_A = 3.619$; $E_A(B_1^-) = 0.392$ from $E_D = 3.227$ eV
$*N_1^\circ + B_1^\circ$	HA, MA, NL, LL, ML	1.893	2.067–2.668	1a–m	1.43	Shells: 1–8, 10, 13, 16, 34, 50/ $E_D + E_A = 3.597$; $E_D(N^\circ) = 3.227$ from $E_A = 0.370$ eV
$*N_1^+ + B_1^\circ$	NA, NL	1.641	1.743–2.180	9a–v	1.53	Shells: 6–10, 12–14, 16, 18, 20, 22, 24, 26, 34, 36, 50, 58, 74, 98, 106, 162/ $E_D + E_A = 3.849$, $E_D(N^+) = 3.479$ from $E_A = 0.370$ eV
$*N_1^{2+} + B_1^\circ$	ML	1.567	1.697–2.417	70a–q	1.52	Shells: 1, 2, 3, 10, 12, 13, 14, 15, 16, 18, 20, 24, 26, 30, 34, 50, 106/ $E_D + E_A = 3.923$, $E_D(N^{2+}) = 3.553$ from $E_A = 0.370$ eV
$*N_2^\circ + B_1^-$	NL	1.890	2.095–2.622	19a–j	1.30	Lines A ($s = 4$), B ($s = 3$) in yellow luminescence/shells: 1, 2, 3, 4, 5, 10, 12, 16, 20, 32/ $E_D + E_A = 3.600$
$*N_2^\circ + B_1^\circ$	NL	1.407	1.798–2.105	20a–g	1.38	Shells: 1, 3, 4, 5–8/ $E_D + E_A = 4.070$; $E_D(N_2^\circ) = 3.700$ from $E_A = 0.370$ eV
$*N_2^+ + B_1^\circ$	NA, MA	3.684	3.865–4.280	67a–i	1.43	Shells: 4, 6, 10, 12, 14, 16, 26, 34, 50/lines of $s = 1–3$ are outside spectrum/ $E_D + E_A = 1.806$; $E_D(N_2^+) = 1.436$ from $E_A = 0.370$ eV
$*N_2^{2+} + B_1^\circ$	NL	2.495	2.649–3.204	18a–g	1.54	Lines C ($s = 50$), D ($s = 32$), E ($s = 20$), F ($s = 2$), H ($s = 1$) in yellow luminescence/shells: 1, 2, 4, 20, 26, 32, 50/ $E_D + E_A = 3.156$; $E_D = 2.786$ from $E_A = 0.370$ eV

DAP: L = limiting energy (different from ZPL), D = dielectric factor

***N₁⁺ + B₁[°] = DAP9:** A set of weak lines is superimposed on the luminescence “B” band of type IIb diamonds. A possible correlation with the N₁⁺ = E = X center has not been investigated.

***N₂[°] + B₁[°] = DAP20:** Some 2–5% of all gem-quality natural diamonds are brown in color. Some of these exhibit bright yellow photoluminescence when excited at 3.40 eV [Col82b]. The infrared absorption spectrum of these diamonds is dominated by the F center lines (V₁N₄ (C₂)_i[°], see Table 8.1.3.6). In addition, lines from A centers (N₂[°]), B centers (V₁N₄), and also from sp²CH₂ (at 182 meV) and sp³CH₂ (at 178 meV) are observed. These latter lines indicate the presence of hydrogen in grain boundaries (see Sect. 9.3). It can be speculated that the grain boundaries stabilize the F centers by blocking the reactions of (9.3b) and (9.4). Superimposed on the broad luminescence bands from the F center (but not related to those) are sets of sharp lines, which belong to DAP18, DAP19, and DAP20. Some lines of DAP18 and DAP19 have been studied under uniaxial stress, and the symmetry of the center (from the dipole orientation) has been determined [Moh82b]. No explanation for the different symmetries was given in the original publication, but a fascinating agreement (and confirmation of the DAP analysis) is obtained when the lattice vectors of the respective DAP are considered (see *N₂⁺ + B₁ = DAP18, below).

***N₂⁺ + B₁[°] = DAP67:** For a general description, see DAP20 above. Two lines are given names [Moh82b]: *A* (*s* = 4) and *B* (*s* = 3). The symmetry of *B* is triclinic in agreement with the lattice vector $\langle 3\ 1\ 1 \rangle$.

***N₂⁺ + B₁[°] = DAP18:** Five lines are given names [Moh82b]: *C* (*s* = 50), *D* (*s* = 32), *E* (*s* = 20), *F* (*s* = 2), *H* (*s* = 1), and *J* (perturbed *s* = 2). The symmetry (obtained from uniaxial stress) for the lines *C*, *D*, *E*, and *J* is C_{2v} with the corresponding lattice vectors C(10, 10, 0), D(8, 8, 0), E(8, 4, 0), and F, J(2, 2, 0). The symmetry of line *H* is trigonal, as expected for the lattice vector $\langle 1\ 1\ 1 \rangle$. Six lines from DAP18 are also observed in absorption (at the same energies as in luminescence, indicating a standard DAP).

***N₂⁺ = DAP4:** When a natural type Ia diamond with $8 \times 10^{19} \text{ cm}^{-3}$ N₂[°] (A center) is irradiated with $1 \times 10^{19} \text{ cm}^{-3}$ neutrons, the DAP4 transitions together with the electronic transition at 1.602 eV of *N₂⁺ are observed. Vibrational sidebands of DAP4 are at 56 meV (typical for N₂, see Table 9.1.5). The acceptor is unknown.

***N₂²⁺ = DAP45:** This center is observed in HTHP synthetic diamond with high nitrogen concentration ($1.3 \times 10^{19} \text{ cm}^{-3}$) after neutron irradiation and 12 h annealing at 800 °C [Vin88b]. The acceptor is unknown; however, the type of spectrum and the hole burning [Sil94a, Sil95] confirm the DAP interpretation.

9.1.6 Discussion

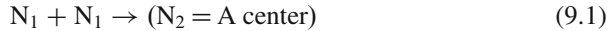
9.1.6.1 Thermally Induced Nitrogen Aggregation in Natural and As-Grown HPHT Synthetic Diamonds

In “newly grown” natural and as-grown HPHT synthetic diamonds, nitrogen is dominantly present in the single substitutional form (N₁[°] = C center, type Ib).

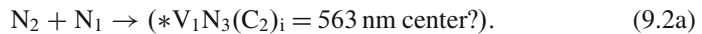
Natural type Ib diamonds are rare, because aggregation occurs under the conditions in the earth's crust.

The sequence of aggregation steps and the structure of the aggregates have been established by annealing experiments [Chr77, Woo86, Kif00] and by theoretical calculations [Mai94]. Triple and quadruple nitrogen centers are stable in natural diamonds only in association with a lattice vacancy [Mai94a].

Step 1: At $T > 1,500^\circ\text{C}$, the single nitrogen starts to migrate, and nitrogen pairs ($\text{N}_2^\circ = \text{A center}$) are formed with an energy gain of 0.5 eV.

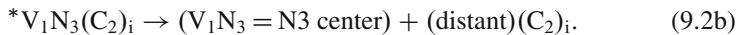


Step 2a: At $T > 1,700^\circ\text{C}$, some of the nitrogen pairs dissociate, while other pairs capture one nitrogen. The triple nitrogen expels a lattice carbon, i.e., a vacancy/interstitial pair is formed.

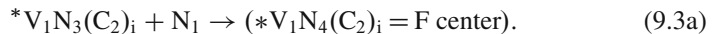


Unfortunately, the $*\text{V}_1\text{N}_3(\text{C}_2)_i$ center is not well documented in the literature. The 563-nm center with absorption and luminescence at 2.202 eV is a possible candidate, due to its great similarity to the N3(a) center at 2.297 eV (see Table 8.2.2).

Step 2b: At the same temperature ($T > 1,700^\circ\text{C}$), the interstitial can leave the $*\text{V}_1\text{N}_3(\text{C}_2)_i$ center, and the N3 center is formed.

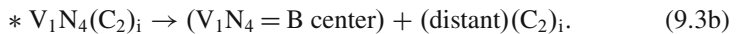


Step 3a: At $T > 1,900^\circ\text{C}$, a further nitrogen is captured and the $*\text{V}_1\text{N}_4(\text{C}_2)_i = \text{F center}$ is formed with a theoretical energy gain of ca. 3 eV [Mai94].

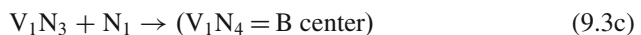


The F center is named after its intense IR absorption bands (see Table 8.1.3.6). Correlated with these IR bands are three ZPL transitions at 2.145, 2.721, and 4.567 eV. The latter is similar to the 4.184–4.197 transitions of the B center (see Sect. 9.1.2 and Tables 8.2.3 and 9.1.4).

Step 3b: At the same temperature ($T > 1,900^\circ\text{C}$), the interstitial can leave the $*\text{V}_1\text{N}_4(\text{C}_2)_i$ center, and a $(\text{V}_1\text{N}_4 = \text{B center})$ is formed.



Step 3c: At the same temperature ($T > 1,900^\circ\text{C}$), the $\text{V}_1\text{N}_3 = \text{N3 center}$ can capture a single nitrogen, and a $\text{V}_1\text{N}_4 = \text{B center}$ is formed with a theoretical energy gain of 3 eV [Mai94].



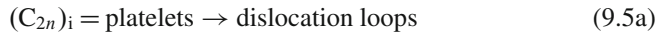
Evidently, there are two possible paths leading to the **B** center formation, depending on whether the $(C_2)_i$ has been released from the $*V_1N_3(C_2)_i$ center ((9.2b), followed by (9.3c)) or not released ((9.3a), followed by (9.3b)). The centers with three nitrogens (**N3** and $*V_1N_3(C_2)_i$) are metastable with respect to the centers with four nitrogens. For this reason, the concentration of the triple nitrogen centers is always very low compared to the centers with one, two, or four nitrogens.

Step 4: The migrating self-interstitials $(C_2)_i$ form planar aggregates called platelets.

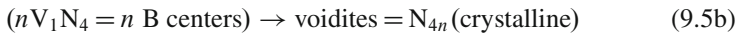


The calibrated absorption of the platelets has been compared with the absorption from **B** centers. In “regular” type IaB diamonds, the absorptions are proportional, while in “irregular” type IaB diamonds, the platelet absorption is very low or absent. A possible explanation can be a partial decomposition (see (9.5a)). An alternate explanation would be that the platelets have never or incompletely been created [Co197].

Step 5a: At still higher temperatures ($T > 2,700^\circ\text{C}$), the platelets decompose, and dislocation loops are formed [Kif00].



Step 5b: At the same temperature ($T > 2,700^\circ\text{C}$), the **B** centers decompose, and voidites are formed. These voidites are octahedral defects consisting of molecular nitrogen in a crystalline form, with dimensions between 2 and 50 nm [Kif00].



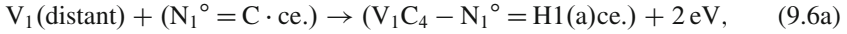
In natural diamonds, all intermediate states of thermal nitrogen aggregation are observed: With single nitrogen (type Ib), with nitrogen pairs (type IaA), with partial transformation from A to B (type IaAB), or with full transformation into the very stable **B** centers (type IaB). Voidites are very rare in natural diamonds.

9.1.6.2 Thermally Induced Nitrogen Aggregation in the Presence of Isolated Vacancies in Irradiated Diamonds

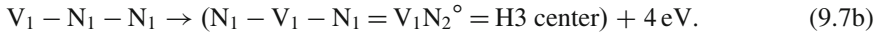
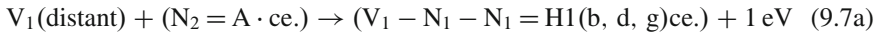
In irradiated diamond, the concentration of isolated *vacancies* can be comparable to the concentration of *nitrogen*. At $T > 600^\circ\text{C}$, the vacancies start to migrate, and can be captured by nitrogen centers with a considerable gain in energy (3.0–6.0 eV) [Mai94a]. The respective reactions are denoted in (9.6a–9.8a). The three associates of a nitrogen center with an *outside* vacancy (**H1(a)** center, **H1(b)** center, and **H1(c)** center) are *metastable* and are *precursors* of the more stable centers **NV** (9.6b), **H3** (9.7b), and **H4** (9.8b). Absorption of the metastable centers is observed in the infrared (see Table A.1.1). This book provides complete assignments for the

H1 lines, especially the **H1**(b,d,g)-DAP30 and **H1**(c,e,f)-DAP31 donor–acceptor transitions (see Sect. 10.1).

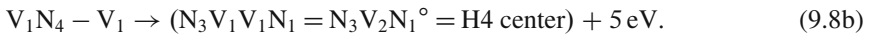
In irradiated diamonds with *isolated nitrogen* (C center), the reactions (9.6a,b) occur after annealing above 600 °C, and the **NV** is formed. The NV center is relatively stable up to temperatures of 1,400–1,700 °C.



In irradiated type IaA diamonds (nitrogen pairs are dominant), the **H3** center is formed by the reactions (9.7a,b)



In irradiated type IaB diamonds (with dominant B centers), the **H4** center is formed by the reactions (9.8a,b)



The precursor centers **H1**(a) in (9.6a), **H1**(b,d,g) in (9.7a), and **H1**(c,e,f) in (9.8a) are metastable and can be observed in absorption (see Tables 8.1.3.1 and 8.1.3.4). Theoretical calculations for the activation energy give 2.4 eV for the reactions of (9.6a), (9.7a), and (9.8a) (vacancy migration) [Mai94a]. The final reordering (site exchange between the vacancy and a carbon or a nitrogen atom) in the reactions of (9.6b), (9.7b), and (9.8b) requires a higher (estimated) activation energy (> 3 eV) with corresponding higher annealing temperatures ($T > 800$ °C) [Mai94a].

9.2 Boron in Diamond

Boron is the second abundant impurity (after nitrogen) in natural diamond. In synthetic diamonds, boron can be introduced as a dopant. In the periodic system, the elements boron and nitrogen are neighbors of carbon, and both can be easily incorporated into the diamond lattice.

Isolated substitutional boron has its ground state 0.37 eV above the valence band. This shallow acceptor center is responsible for the p-type semiconductor character of type IIb diamonds (where the concentration of compensating donors is lower than the boron concentration).

There are six types of boron centers in diamond. The majority (3–5) contains intrinsic defects, which dominantly determine the properties (see Chap. 8):

1. Isolated substitutional boron: The B_1° acceptor (see Table 9.2.1).
2. Standard DAP of boron with nitrogen = DAP1 (see Table 9.1.5) or with phosphorous = DAP2 (see Table 9.2.2).
3. Associate with a lattice vacancy (see Table 8.1.7.1).
4. Associates of B_1 , B_2 , or B_3 with the $\langle 1\ 0\ 0 \rangle$ $(C_2)_i$ split interstitial (see Table 8.2.3).
5. Associates of B_1 with the $\langle 1\ 0\ 0 \rangle$ (N_1C_1) split interstitial in three charge states (see Tables 8.2.4).
6. Boron-bound exciton lines (see Table 9.2.6).

9.2.1 Isolated Substitutional Boron

The absorption spectrum of B_1° was explained by a calculation, using effective mass theory [Cro67b]. The ground state is 0.372 eV above the valence band, and the transitions to the excited states occur at 0.2680–0.3646 eV (see Table 9.2.1). The three most intense transitions (at 0.3042, 0.34710, and 0.36273 eV) have sidebands with one to three phonons of energy 161 meV. This LVM frequency is close that of the fundamental lattice phonon (165 meV), indicating a slightly lower force constant for the B–C, compared to C–C stretch vibration.

An interesting phenomenon is observed in the photoconductivity spectrum (at 120 K). The so-called photothermal ionization process (photon + thermal phonon) explains the photoconductivity peaks well below the ionization threshold (these peaks coincide with the absorption peaks) [Col68].

9.2.2 Standard DAP of Boron with Nitrogen (DAP1, 9, 18, 19, 20, 67, 70), Phosphorous (DAP2), or Oxygen (DAP17)

The nitrogen containing centers (DAP1, 9, 18, 19, 20, 67, 70) are already listed and described in Table 9.1.5, Sect. 9.1.5. Other data are collected in Table 9.2.2.

In samples which contain boron and phosphorous (as evidenced by their respective bound excitons), 23 lines in the range 4.711–5.275 eV are observed, arising from the $B_1^\circ + P_1^\circ - \text{DAP2}$ transitions [Ste99a,b]. The large number of resolved DAP lines has probably to do with the fact that both impurities have shallow states in the bandgap: $E_D(P) = E_c - 0.620$ eV, and $E_A(B) = E_v + 0.370$ eV, with a corresponding large Bohr radius, leading to a better overlap than for the deep donor nitrogen ($E_D(N) = 3.230$ eV).

Table 9.2.1 Absorption and photoconductivity lines from the substitutional single boron in diamond (after [Smi62, Cro67b, Wal79, Zai01])

Line ^a	Observed	(meV)	Assigned ^b	I-II ^c	Name/comment
LVM	NA, HA, MA	159.8	LVM	–	B–C stretch
B'	PC ^e	268.0	I/II → 1	–	1s(Γ_7/Γ_8) → 2s (forbid- den); 2 SBs
B(a)	NA	304.2	I/II → 2	–	1s(Γ_7/Γ_8) → 2p (Γ_6/Γ_8)
B(b)	NA	335.6	II → 3	–	1s(Γ_7) → 2p (Γ_8)
B(c)	NA	337.3	I → 3	(1.7)	1s(Γ_8) → 2p (Γ_8)
<i>B(d)</i> ^f	NA	340.4	–	–	–
B(e)	NA	341.48	II → 4	–	1s(Γ_7) → 2p (Γ_8)
<i>B(f)</i> ^f	NA	342.10	–	–	–
B(g)	NA	343.53	I → 4	2.05	1s(Γ_8) → 2p (Γ_8)
<i>B(h)</i> ^f	NA	345.1	–	–	–
<i>B(i)</i> ^f	NA	346.37	–	–	–
B(j)	NA, HA, LA	347.10	II → 5	–	1s(Γ_7) → 2p (Γ_6)
B(k)	NA	349.13	I → 5	2.03	1s(Γ_8) → 2p (Γ_6)
B(l)	NA	352.4	II → 6	–	1s → 2p
B(m)	NA	354.56	I → 6	(2.2)	1s → 2p
B(n)	NA	355.79	II → 7	–	1s → 2p
B(o)	NA	357.89	I → 7	2.10	1s → 2p
B(p)	NA, HA, LA, MA	362.73	II → 8	–	1s → 2p
B(q)	NA	364.6	I → 8	(1.9)	1s → 2p
<i>E_A</i>	NA, HA, LA, MA, PC	372	I/II → VB	–	Ionization energy
B'-s1	PC	430	B' + 0.162	–	SB (1 × 162 meV) ^d
B(a)-s1	NA, HA, LA	466	B(a) + 0.162	–	SB (1 × 162 meV)
B(j)-s1	NA, HA, LA	508	B(j) + 0.161	–	SB (1 × 161 meV)
B(p)-s1	NA, HA, LA	527	B(p) + 0.164	–	SB (1 × 164 meV)
B'-s2	PC	591	B' + 324	–	SB (2 × 162 meV)
B(a)-s2	NA, HA, LA	625	B(a) + 0.321	–	SB (2 × 161 meV)
B(j)-s2	NA, HA, LA	670	B(j) + 0.323	–	SB (2 × 161 meV)
B(p)-s2	PC	686	B(p) + 0.323	–	SB (2 × 162 meV)
B(a)-s3	PC	790	B(a) + 0.486	–	SB (3 × 162 meV)
B(j)-s3	NA, HA, LA	830	B(j) + 0.483	–	SB (3 × 161 meV)

(continued)

Table 9.2.1 (continued)

Line ^a	Observed	(meV)	Assigned ^b	I-II ^c	Name/comment
B(p)-s3	PC	850	B(p) + 0.487	–	SB (3 × 162 meV)
B(a)-s4	PC	953	B(a) + 0.649	–	SB (4 × 162 meV)
B(p)-s4	PC	1,015	B(p) + 0.652	–	SB (4 × 163 meV)
B(p)-s5	PC	1,180	B(p) + 0.817	–	SB (5 × 163 meV)

^aBold = intense line;^bI, II = 1s ground state (2.06 meV splitting); 2–8 = excited 2p states^cDifference, arising from 2.06 meV gr. st. splitting;^dLVM frequency is 160 meV in the ground state (see line 1) and 162 meV in the excited state (see sidebands)^eIndirect observed;^fAdditional lines from 19% ¹⁰B or disturbed boron**Table 9.2.2** DAP of boron with phosphorous [Ste99a, b] or with oxygen [Rua93a]

Defect	Observed	<i>L</i> (eV)	Lines (range) (eV)	Standard DAP	<i>D</i> (eV)	Comment
*B ₁ ^o + P ₁ ^o	HL, LL	4.500	4.711–5.275	2a–w	+1.72	Shells: 3, 5, 9, 11, 12, 14, 15, 16, 17, 18, 19, 20, 22, 24, 25, 26, 30, 31, 32,37, 39, 50/ <i>E</i> _D + <i>E</i> _A = 0.990; <i>E</i> _D (P) = 0.620 from <i>E</i> _A = 0.370 eV
*B ₁ ^o *O ₁ ^o	LL	2.534	2.676–2.725	17a–g	+1.29	Shells: 34, 44, 48, 50, 58, 62/ <i>E</i> _D + <i>E</i> _A = 2.956; <i>E</i> _D (O) = 2.586 from <i>E</i> _A = 0.370 eV

For boron with nitrogen (six centers), see Table 9.1.5

DAP: *L* = limiting energy (no ZPL for standard DAP), *D* = dielectric factor

9.2.3 Associate of Boron with a Lattice Vacancy

There are two transitions with ZPLs at 2.395 eV (*V₁B₁(a)^o) and 3.120 eV (*V₁B₁(b)^o) (see Table 8.1.7.1) The sideband DAPs are seen as structure on broad bands. The ZPL at 2.395 eV is weak in X-ray luminescence but is intense in photoluminescence. The observed QLVM has *f* = 50 and *w* = 25 meV, which

can be tentatively assigned to $^{11}\text{B}_1^{12}\text{C}_3$ with calculated values $f = 50.4$ and $w = 27.0$ meV (the natural abundance of the boron isotopes is $^{11}\text{B}/^{10}\text{B} = 81/19\%$).

9.2.4 Associates of B_1 , B_2 , or B_3 with the $\langle 100 \rangle (C_2)_i$ Split Self-interstitial

These centers are named 2BD (type **IIb** damaged) and are listed in Table 8.2.3. The lines from $^*(C_2)_iB_2^\circ - \text{DAP97}$ transitions are weak, and no other 2BD–DAP transitions are observed.

9.2.5 Associates of B_1 with the $\langle 100 \rangle$ Split $(N_1C_1)_i$ Interstitial in Three Charge States

A short discussion of these centers is given in Sect. 8.2.4. In as-grown CVD synthetic diamonds, boron (identified by its bound exciton) can be present by intentional doping or by unintentional transfer from the boron-doped silicon substrate [Ste96a]. In the cathodoluminescence (CL) of such samples, the lines of $V_1N_1^\circ$ at 2.154 eV, $^*(C_2)_iN_1^-$ at 3.188 eV, and $^*(C_2)_iN_1^\circ (= 5\text{RL})$ at 4.582 eV are observed, together with a group of nine lines at 2.417–2.792 eV [Ste96a]. These latter lines are typical DAP transitions, which can be tentatively assigned to $^*(N_1C_1)_iB_1^\circ$ with the ZPL at 2.792 eV, and the sideband DAP99 (see Table 8.2.4).

In similar CVD samples, CL, lines of $^*(C_2)_iN_1^-$ at 2.807 eV, and $^*(N_1C_1)_i^\circ$ at 3.188 eV and lines from DAP1 ($= ^*N_1^\circ + B_1^\circ$; 2.067–2.668 eV) are observed, together with a group of nine lines at 2.725–3.092 eV [Col89c, Dis94a]. This group of lines is tentatively assigned to $^*(N_1C_1)_iB_1^+$ with the ZPL at 3.092 eV, and the sideband DAP100 (Table 8.2.4).

In a boron-doped hot filament grown CVD sample, the $(N_1C_1)_iB_1$ center is probably observed in three charge states: Weak ZPLs at 2.792 eV (from $^*(N_1C_1)_iB_1^\circ$) and 3.092 eV (from $^*(N_1C_1)_iB_1^+$), and an intense group of eight lines at 2.330–2.992 eV, which can be tentatively assigned to $^*(N_1C_1)_iB_1^-$ with the ZPL at 2.992 eV, and the sideband DAP101 (Table 8.2.4).

9.2.6 Boron-Bound Exciton Lines

Cathodoluminescence lines from the boron bound exciton are listed in Table 9.2e. The spectrum is typical for a shallow defect center in diamond. The ionization energy (E_i) is 370 meV, and the binding energy (E_b) is 51 meV, in excellent agreement with Haynes' rule, which predicts $E_i/E_b = 7$ [Ste99a].

Table 9.2.6 Cathodoluminescence lines from boron-bound exciton (BE) transitions in diamond (after Figs. 5.152, 5.169, 7.157 [Dea65b, Ste97b, Ruf98, Zai01])

Line [Dea65]	Assignment	Relat. int.	Observed	(eV)	Diff. (meV) ^a	Name/comment (SB difference in meV) ^b
D ₀ '	BE-B(b)	1	NL, HL, LL	5.3671	–	No phonon BE; weak SBs at 5.3652(–1.9 meV), 5.3693(+2.2), 5.2709(+3.8) ^b
D ₀	BE-B(a)	2	NL, HL, LL	5.3558	–11 ^c	No phonon BE; weak SBs at 5.3539 (–1.9 meV), 5.3575(+1.7), 5.3590(+3.2) ^b
D ₁ '	B(b)-1Ph	5	NL	5.227	–140	TO phonon
D ₁	B(a)-1Ph	9	NL, HL, LLML	5.215	–141	TO phonon
D ₁ ''	B(a)-1Ph	1	NL, HL, LL, ML	5.193	–163	LA/LO phonon
D ₂ '	B(b)-2Ph	6	NL,HL,LL	5.060	–307	165(LO) + 142(TO)
D ₂	B(a)-2Ph	5	NL, HL, LL, ML	5.048	–308	165(LO) + 143(TO)
D ₂ ''	B(a)-2Ph	1	NL	5.023	–333	(2×) 162(LO)
D ₃ '	B(b)-3Ph	3	NL	4.903	–464	(2×) 162(LO) +140(TO)
D ₃	B(a)-3Ph	2	NL	4.890	–466	(2×) 163(LO) +140(TO)
D ₄	B(a)-4Ph	2	NL	4.755	–601	(2×) 161(LO) + (2×) 140(TO)

^aLattice phonons which couple to the free exciton are 87(TA), 141(TO), and 163(LA/LO) meV

^bSplitting of –1.9 meV from split acceptor ground state (see Table 9.2.1), and of +3.3 meV from initial bound exciton state [Ste97b, Ruf98]

^cSplitting of –11 meV from spin–orbit splitting of the valence band

It may be mentioned that similar bound exciton spectra are observed for phosphorous ($E_i = 620$, $E_b = 88$ meV) [Ste99b] and for lithium ($E_b = 130$ meV) [Zai97a] (see Tables 5.3.12.1–5.3.12.2).

9.2.7 Discussion

The blue color of natural diamonds (all of type IIb) is caused by boron. It has been reported that the so-called Cape yellow diamonds exhibit bright blue luminescence when excited in the ultraviolet [Col82b].

In boron-doped synthetic diamonds, the ultraviolet absorption from daylight causes a bright blue color, and this has been used for some commercial applications.

9.3 Hydrogen in Diamond

Hydrogen in diamond is of special interest because of the following:

1. Synthetic CVD diamond is usually grown in a hydrogen-rich atmosphere.
2. Passivation of the surface has been observed [Dav94a].
3. A possible passivation of donors and acceptors has been discussed [Dav94b].
4. Several spectral lines from hydrogen centers have been observed in different classes of diamond.

In most natural type Ia diamonds, absorption lines from C–H vibrations of the $^*(V_1H_1)^\circ$ center are observed, with two sharp fundamental lines and seven sidelines (see Sect. 9.3.1 and Table 9.3.1).

In the grain boundaries of polycrystalline (heteroepitaxial or homoepitaxial) CVD diamond, 18 absorption lines from C–H bend vibrations (Table 9.3.2) and 11 lines from C–H stretch vibrations (Table 9.3.3) are observed. It is remarkable that these frequencies are essentially identical with those from C–H vibrations in (amorphous) diamond-like carbon (DLC). However, the line width for the hydrogen lines in the grain boundaries and in DLC is considerably larger (0.4–15%), compared to 0.1% for the $^*(V_1H_1)^\circ$ center in the diamond crystal (see Tables 9.3.1–9.3.3).

In ion-implanted diamond, a luminescence line is observed at 2.272 eV for protons (Table 5.3.7.3) and at 2.274 eV for deuterons (Table 7.1) [Gip83]. The frequency shift is within experimental error, and is no proof for hydrogen involvement.

Several other lines in diamond, which in the literature are ascribed to hydrogen, are marked by “H?” in Tables 2.1.1.1–7.4.

9.3.1 Hydrogen Lines in Natural Diamond

Natural C–H lines. In Table 9.3.1, two main absorption lines at 174.2 and 385.2 meV together with seven sidelines are listed. These lines have been observed in bulk natural diamond (mainly of type Ia) [Cha59, Woo83], [Dav84b], [Fri91a] and also in natural diamond “coat” [Run71]. Confirmation of the line assignment to the fundamental bend and stretch vibrations of C–H came from a careful analysis of the sidelines. Especially, the weak line at 0.3841 eV from the 1.1% abundant ^{13}C isotope ruled out an N–H vibration [Woo83]. The six other sidebands are overtones or combinations of the fundamental vibrations [Dav84, Fri91]. Remarkable are the anharmonicities (including level mixing and repulsion) of up to 2.3%. All C–H lines in Table 9.3.1 originate from the same center, as confirmed by a correlation factor 0.97–0.99 for the intensities of the five dominant lines, tested on seven samples [Dav84].

From the experimental observations and the data listed in Table 9.3.1, the following conclusions can be drawn:

Table 9.3.1 C-H and N-H vibrational lines from three centers in *natural* diamond, $^*(V_1H_1)^\circ$, $^*(V_1H_1)N_1^\circ$, and $^*(V_1H_1)N_4^\circ$, and one center in *non-natural* (modified or CVD) diamond, $^*(V_1H_1)N_3^\circ$

Line	Energy (meV)	Frequ. (cm^{-1})	Width (%)	Relat. int. (%) ^a	Assignment	Anharm. shift (%)	Fig. [Zai01]	References
<i>Natural</i>								
$^*(V_1H_1)^\circ$								
NA0174a	174.2	1,405	0.11	20	C-H bend = b	-	3.8	[Dav84b]
NA0174a-s1	345.4	2,786	0.09	3	2b	-0.9	3.7	[Dav84b]
i13-NA0174b	384.1	3,098	0.09	1.4	¹³ C-H (s)	-	-	[Dav84b]
NA0174b ^b	385.2	3,107	0.09	100	C-H str. = s	-	3.7	[Woo83]
NA0174a-s2	516.7	4,168	0.11	0.6	3b	-1.1	3.5	[Dav84b]
NA0174b-s1	557.8	4,499	0.11	5	1s + 1b	-0.3	3.5	[Dav84b]
NA0174a-s3	688.7	5,555	-	0.04	4b	-1.2	3.5	[Fri91a]
NA0174b-s2	729.0	5,880	-	0.06	1s + 2b	-0.6	3.5	[Fri91a]
NA0174b-s3	752.5	6,070	-	0.4	2s	-2.3	3.5	[Fri91a]
$^*(V_1H_1)N_1^\circ$								
NA0182a	182.2	1,470	-	-	N-H bend = b	-	3.13	[Che94b]
NA0182a-s1	362.0	2,920	-	-	2b	-0.7	3.26	[Fri91a]
NA0182b	401.2	3,236	-	-	N-H str. = s	-	3.7	[Fer96]
NA0182b-s1	583.2	4,704	-	-	1s + 1b	-0.1	3.5	[Fri91a]
$^*(V_1H_1)N_4^\circ$								
NA0192a	191.8	1,547	-	-	N-H bend	-	3.7	[Fer96]
NA0192b	423.8?	3,418	-	-	N-H stretch	-	3.7	[Fer96]?
<i>Non-natural</i>								
$^*(V_1H_1)N_3^\circ$								
MA0198a	198.4	1,600	-	-	N-H bend	-	3.13	[Che94b]
LA/MA0198b	390.5	3,150	-	-	N-H stretch	-	3.13	[Che94b, Mill95]

^aFor the relative intensities, the strongest line was fixed at 100%

^bThe 385 meV line is the ZPL of DAP41a-e (see Table 2.1.1.1)

1. The center has rotational symmetry, because there is only one (doubly degenerate) bending vibration.
2. The hydrogen is bonded to only one carbon, because the relative intensity of the $^{13}\text{C}\text{-H}$ line at 384.1 meV is 1.4%, which is much closer to the value 1.1% (for bonding to one carbon) than to a value of 2.2% (for bonding to two carbons). The observed isotope shift is -0.29% , which is close to the theoretical shift (0.30%, calculated from (11.1) with $\alpha = 1$).
3. The observation of certain overtones (e.g., $2\times$ bend at 345.4 meV) unambiguously rules out inversion symmetry for the center (from group theory) [Dav84b]).
4. The C–H bond must be of a rather unusual nature, because the frequency is 6.6% higher than for a normal sp^3CH_1 bond (Table 9.3.3), and because the relatively high intensities and large anharmonic shifts of the overtone or combination vibrations are rather unexpected.

The best agreement with the above observations is obtained by a configuration of a “hydrogen-terminated carbon atom at some form of lattice imperfection” [Dav94b]. It can now be taken as granted that this lattice imperfection is a carbon vacancy, filled with one hydrogen and denoted by $^*(\text{V}_1\text{H}_1)$. This interpretation is strongly supported by the similarity with the newly identified $^*(\text{V}_4\text{H}_4)$ center in homoepitaxial CVD diamond (see Sects. 9.3.6 and 10.1). The C–H stretch frequency for the $^*(\text{V}_4\text{H}_4)$ center at 387.3 meV [Fuc95b] is 0.5% higher than for the $^*(\text{V}_1\text{H}_1)$ center. Both stretch vibrations have very similar sidebands from coupling to DAP transitions [Dis03] (see $^*(\text{V}_4\text{H}_4)\text{b-DAP40}$ and $^*(\text{V}_1\text{H}_1)\text{b-DAP41}$ in Table 10.1).

It should be mentioned that the bond center position (between two carbon atoms) is evidently preferred by the (extremely short-lived) “anomalous” muonium [Est87]. For the long-lived hydrogen center in Table 9.3.1, the bond center position can be ruled out by the observations (2) and (3) above.

Natural N–H lines. In Table 9.3.1, three centers with N–H bend and stretch vibrations are listed, two $^*(\text{V}_1\text{H}_1)\text{N}_1^\circ$ and $^*(\text{V}_1\text{H}_1)\text{N}_4^\circ$ in natural and one $^*(\text{V}_1\text{H}_1)\text{N}_3^\circ$ in non-natural diamond. The intensity of these lines is not directly correlated with those of the $^*(\text{V}_1\text{H}_1)^\circ$ center. The three centers are observed in diamonds with a high concentration of hydrogen and nitrogen, and can therefore be assigned to N–H vibrations, i.e., the hydrogen is in a slightly different environment. Note that the N–H vibrational stretch energies are higher than the respective energies for C–H vibrations. The difference is 4.5% for $^*(\text{V}_1\text{H}_1)\text{N}_1^\circ$, 1.8% for $^*(\text{V}_1\text{H}_1)\text{N}_3^\circ$, and 10% for $^*(\text{V}_1\text{H}_1)\text{N}_4^\circ$.

9.3.2 Hydrogen Bend Lines in Polycrystalline CVD Diamond

The hydrogen content in polycrystalline CVD diamond is relatively high, reaching up to 20 at. % H in heteroepitaxial films [Dis93] and up to 3.3 at. % H in homoepitaxial films [Jan92]. It was shown by electron probe microanalysis that the hydrogen is predominantly located in the *diamond grain boundaries* (DGB), which

consist of disordered amorphous carbon [Fal93]. Independently, this conclusion was drawn from the similarity between the C–H vibrational absorption lines in polycrystalline CVD diamond and in amorphous DLC [Dis93] (see also Tables 9.3.1–9.3.4). The lines in Tables 9.3.1–9.3.4 are positively identified as C–H vibrations by the observed isotope shift for $^1\text{H}/^2\text{D}$ and $^{12}\text{C}/^{13}\text{C}$ substitution [Dis87, Dis92, Fuc95b].

In Table 9.3.2, the 18 infrared absorption lines from C–H bend vibrations are listed. These relatively broad lines are observed in the range 80–190 meV ($680\text{--}1,500\text{cm}^{-1}$). In some samples, there is overlap with the defect-induced one-phonon absorption of crystalline diamond in the range 70–170 meV ($550\text{--}1,350\text{cm}^{-1}$), and of C–C vibrational absorption lines in the range 100–270 meV ($840\text{--}2,180\text{cm}^{-1}$). Because of these overlaps and of the broadness, the C–H bend lines are less well documented than the C–H stretch lines. There exists a qualitative intensity correlation between bend and stretch vibrations for the eight different C–H configurations listed in Tables 9.3.1–9.3.4.

9.3.3 Hydrogen Stretch Lines in Polycrystalline CVD Diamond

In Table 9.3.3, the 11 infrared absorption lines from C–H stretch vibrations are listed. The spectra consist of partly overlapping lines in the range 350–410 meV ($2,820\text{--}3,330\text{cm}^{-1}$). After early reports [Wil89, Bi.90, Jan91], deconvolution of the overlapping lines [Dis87, Dis92, Dis93, Joh94] allowed a quantitative analysis and the assignment to the configurations given in Tables 9.3.3 and 9.3.4.

Of special interest is the line at 349.9 meV ($2,822\text{cm}^{-1}$) [Dis93], which is completely absent in DLC [Dis87] (see Table 9.3.3). On the contrary, a single sharp (0.3% width) C–H stretch line at 350.9 meV ($2,830\text{cm}^{-1}$) was observed for a hydrogen monolayer on a diamond (111) cleavage plane [Chi92]. Therefore, a common configuration for both lines can be assumed, i.e., a single hydrogen atom, bonded to a tetrahedral lattice carbon, denoted by “lattice sp^3CH_1 .” The intensity of this C–H stretch line correlates with that of the relatively sharp C–H bend line at 155.2 meV ($1,252\text{cm}^{-1}$) in Table 9.3.2 [Jan92].

This new “lattice sp^3CH_1 ” line, together with the ten lines from the seven traditional C–H configurations (*aliphatic* sp^3CH_3 , sp^3CH_2 , sp^3CH_1 , *olefinic* sp^2CH_2 , sp^2CH_1 , *aromatic* sp^2CH_1 , and *acetylenic* sp^1CH_1), has been observed in CVD diamond (see Tables 9.3.1–9.3.4). However, the acetylenic line from sp^1CH_1 at 412 meV ($3,323\text{cm}^{-1}$) is absent in most samples, except in homoepitaxial CVD diamond from microwave deposition [Dis92, Fuc95b].

9.3.4 Abundances of C–H Configurations

From the absorption intensities, the abundances of the different C–H configurations and the total hydrogen content can be derived. In Table 9.3.4, the percentages of

Table 9.3.2 C–H bend vibrational absorption lines, observed in the diamond grain boundaries (DGB) of polycrystalline (heteroepitaxial or homoepitaxial) CVD diamond; in natural brown diamond (NBD), in natural gray diamond (NGD), in amorphous diamond-like carbon (DLC), and in polymer-like amorphous carbon (PAC) (see also Table 6.1.1.1)

Line	Assessment		Diamond: DGB, NBD, NGD				DLC		PAC	
	Configuration ^c	Sym. ^d	Energy (meV)	Frequ. (cm^{-1})	Width ^b (%)	Refs.	Energy (meV)	Energy (meV)	Energy (meV)	Refs.
RA0085a1	sp ³ CH ₃ aliph.	C _{3v} : A ₂ C _{2v} : B ₁	(34.1) 85.17	(275) 687	Torsion ^e 1–7	(predicted) [Rei98]	(34.1) 86.8	(34.1) 86.8	(34.1) 86.8	[Dis87] [Dis87]
RA0087a	sp ³ CH ₂ acetyl.	C _{∞v} : E	–	–	–	–	–	–	86.8	[Dis87]
RA0088a1	olef. sp ² CH ₂	C _{2v} : B ₁	88.02	710	13–15	[Fri91a]	–	–	86.8	[Dis87]
RA0095a1	arom. sp ² CH ₁	C _s : B	95.50	770	12–14	[Fri91a]	93.6	93.6	93.6	[Dis87]
RA0108a1	olef. sp ² CH ₁	C _s : B	107.9	870	2–7	[Fri91a]	104.1	104.1	104.1	[Dis87]
RA0088a2	olef. sp ² CH ₂	C _{2v} : A ₂	114.1	920	4–6	[Che92b]	112.8	112.8	112.8	[Dis87]
RA0085a2	aliph. sp ³ CH ₂	C _{2v} : B ₂	125.2	1,010	2–6	[Fri91a]	127.7	127.7	127.7	[Dis87]
RA0133a1	aliph. sp ³ CH ₃	C _{3v} : E	133.3	1,075	3–5	[Che92b]	–	–	133.3	[Dis87]
RA0088a3	olef. sp ² CH ₂	C _{2v} : B ₂	137.6	1,110	2–6	[Jan92]	–	–	137.6	[Dis87]

RA0085a3	aliph. sp ³ CH ₂	C _{2v} : A ₂	145.1	1,170	1-5	[Rei98]	145.1	146.3	[Dis87]
LA0155a	lattice sp ³ CH ₁ ?	C _{3v} : E	155.2	1,252	1-2	[Jan92]	(not obs.)	—	—
RA0108a2	olef. sp ² CH ₁	C _S : A	159.9	1,290	5-7	[Jan91]	159.9	158.7	[Dis87]
RA0133a2	aliph. sp ³ CH ₃	C _{3v} : A ₁	164.9	1,330	2-4	[Jan91]	—	164.3	[Dis87]
RA0171a	aliph. sp ³ CH ₁	C _{3v} : E	171.1	1,380	4-6	[Che94b]	169.8	—	[Dis87]
RA0095a2	arom. sp ² CH ₁	C _S : A	177.3	1,430	1-2	[Fri91a]	177.9	179.1	[Dis87]
RA0085a4	aliph. sp ³ CH ₂	C _{2v} : A ₁	178.5	1,440	4-7	[Jan91]	178.5	179.8	[Dis87]
RA0088a4	olef. sp ² CH ₂	C _{2v} : A ₁	181.6	1,465	2-4	[Jan91]	—	179.8	[Dis87]
RA0133a3	aliph. sp ³ CH ₃	C _{3v} : E	185.3	1,495	1-3	[Fri91a]	—	184.7	[Dis87]

^a Assignment from [Dis85, Dis87]

^b Width (sample dependent; range)

^c Configuration: *aliph.* aliphatic, *acetyl* acetylenic, *olef* olefinic, *arom* aromatic

^d *Sym.* Symmetry

^e Torsion: IR-inactive

Table 9.3.3 C–H stretch vibrational absorption lines (LA, MA, and RA), observed in diamond grain boundaries (DGB) of polycrystalline (heteroepitaxial or homoepitaxial) CVD diamond, in natural brown diamond (NBD), in natural gray diamond (NGD), in amorphous diamond-like carbon (DLC), and in PAC. Four MA lines are observed from hydrogen-covered diamond crystal surface (HCS)

Line	Assignment	Diamond: DGB, NBD, NGD, HCS						DLC		PAC		
		Configuration	Sym.	Energy (meV)	Fr. (cm^{-1})	Wi. (%)	R. i. (%)	Ref.	Energy (meV)	Wi. (%)	Energy (meV)	Refs.
LA0155b	Lattice $sp^3 CH_1?$	$C_{3v} : A_1$		349.9	2,822	0.4–1.6	1–24	[Dis93]	absent	–	–	absent
MA0155b	HCS, see Table	$C_{3v} : A_1$		350.2	2,825	–	–	[And94]	–	–	–	–
RA0085b1	5.1.2.2 aliph. $sp^3 CH_2$	$C_{2v} : A_1$		353.3	2,850	0.7–2.1	5–38	[Dis93]	353.3	2.7	353.3	[Dis87]
MA0085b1	HCS, see Table 5.1.2.2	$C_{2v} : A_1$		354.2	2,857	–	–	[Chi92]	–	–	–	–
RA0133b1	aliph. $sp^3 CH_3$	$C_{3v} : A_1$		356.4	2,875	1.0–2.9	1–20	[Dis93]	–	–	356.4	[Dis87]
MA0133b1	HCS, see Table 5.1.2.2	$C_{3v} : A_1$		358.9	2,895	–	–	[And94]	–	–	–	–

RA0171b	aliph. sp ³ CH ₁	C _{3v} : A ₁	361.3	2,914	0.5–1.8	1–35	[Dis93]	362.0	3.0	–	[Dis87]
RA0085b2	aliph. sp ³ CH ₂	C _{2v} : B ₁	361.6	2,917	0.9–2.1	5–38	[Dis93]	362.0	3.0	362.0	[Dis87]
RA0133b2	aliph. sp ³ CH ₃	C _{3v} : E	367.8	2,967	1.2–2.9	2–30	[Dis93]	–	–	365.1	[Dis87]
MA0133b2	HCS, see Table 5.1.2.2	C _{3v} : E	366.4	2,955	–	–	[And94]	–	–	–	–
RA0088b1	olef. sp ² CH ₂	C _{2v} : A ₁	368.5	2,972	0.5–1.2	0–10	[Dis93]	–	–	368.2	[Dis87]
RA0108b	olef. sp ² CH ₁	C _s : A	371.9	3,000	0.9–2.3	0–8	[Dis93]	371.9	2.6	371.9	[Dis87]
RA0088b2	olef. sp ² CH ₂	C _{2v} : B ₁	375.0	3,025	0.8–1.2	0–10	[Dis93]	–	–	375.0	[Dis87]
RA0095b	arom. sp ² CH ₁	C _s : A	378.1	3,050	1.1–2.3	0–11	[Dis93]	377.5	2.2	379.4	[Dis87]
RA0087b	acetyl. sp ¹ CH ₁	C _{∞v} : A	412.0	3,323	0.5–0.7	0–11	[Dis92]	409.1	1.3	409.1	[Dis87]
NA0087b ¹	acetyl. sp ¹ CH ₁	C _{∞v} : A	412.0	3,323	0.2	–	[Woo83]	–	–	–	–

F: frequency, *W*: width (sample dependent), *R. i.* relative intensity (sample dependent), *Sym.* symmetry, Configuration: *aliph.* aliphatic, *acetyl.* acetylenic, *olef.* olefinic, *arom.* aromatic,
¹ After natural irradiation (see Table 2.1.2.2)

the eight configurations are listed for 19 different types of samples. The results are clearly sample dependent. Without going into details, it is clear that several interesting conclusions may be drawn from the data, and these can possibly contribute to a better understanding of the growth mechanism and texture development [Wil94, Mül96]. It may also give more insight into the structure of the grain boundaries [Fal93]. A brief discussion on the sample dependence is given below.

No. 1, 2: Increasing the hydrocarbon content in the feed gas of hot-filament deposited heteroepitaxial CVD diamond from 1% (HF-1%-CH) to 5% (HF-5%-CH) leads to a 50 times higher hydrogen content (due to smaller grains) [Dis93].

No. 3–6: Different substrates were used in a simultaneous microwave CVD deposition experiment. The label MW-Si denotes heteroepitaxial CVD on silicon, and MW-100, MW-110, and MW-111 denote homoepitaxial CVD on (1 0 0), (1 1 0), and (1 1 1) diamond substrates [Dis92].

No. 7–10: A set of flame-grown homoepitaxial CVD samples was deposited on (1 0 0), (1 1 0), and (1 1 1) diamond substrates. The deposition temperature was 930–1,020 °C, except for the high temperature sample (FL-111-HT) with 1,120 °C [Jan92].

No. 11, 12: The influence of nitrogen addition in the feed gas was studied in microwave CVD deposition with 0% and 1% nitrogen gas [Dis92].

No. 13, 14: The application of a negative DC bias (0 and 250 V) during microwave CVD deposition leads to a remarkable increase in sp^2 hybridization from 1% to 11% [Joh94].

No. 15, 16: After heat treatment at 1,475 °C of a hot-filament deposited CVD film, considerable modification of the C–H configurations was observed [Dis92].

No. 17–19: For comparison, some results from DLC (as-grown and heat treated for 4 h at 600 °C) [Dis83] and from polymer-like amorphous carbon (PAC) [Dis87] are included in Table 9.3.4. Remarkable is the high sp^2 percentage in as-grown samples (30–45%) and the complete transformation into aromatic sp^2 (from 8% to 98%) after the above-mentioned heat treatment.

The average C–H hybridization for the 16 CVD diamond samples in Table 9.1.4 is given below line 16: $sp^3 : sp^2 : sp^1 = 88 : 11 : 1\%$. The dominant configuration is sp^3CH_2 (average 47%). Exceptions with a different dominant configuration are sp^3CH_3 in (HF-1%-CH, MW-0-Volt) or sp^3CH_1 in (FL-100-diam., HF-H-1475).

The results in Table 9.3.4 for the hybridization of the C–H bonds are also representative for the hybridization of the C–C bonds in the amorphous carbon network (Table 9.3.5). This has been confirmed by electron energy loss spectroscopy for DLC [Fin84] and also by Raman spectroscopy for polycrystalline (CVD) diamond [Wag89] and amorphous DLC [Dis85, Wag89].

9.3.5 Frequencies of C–C Vibrations from H-Bonded Carbon

The atoms from the carbon network which are bonded to hydrogen show characteristic infrared-active C–C vibrations. These lines (see Table 9.3.6) are observed in natural diamond coat (NDC), DLC, and PAC. Discrimination against the C–H

Table 9.3.4 Abundances of C–H configurations in DGB, in polycrystalline (heteroepitaxial or homoepitaxial) CVD diamond (Nos. 1–16), in amorphous diamond-like carbon (DLC, Nos. 17, 18), and in PAC (No. 19), as obtained from deconvoluted C–H stretch lines

Nos.	Sample	Film thickness (μm)	Hydro-gen (at%)	aliph. sp ³		aliph. sp ³		latt. sp ³	total sp ³ (%)	olef. sp ²		olef. sp ²	arom. sp ²		Total sp ²	acetyl. sp ¹	Refs.
				CH ₃ (%)	CH ₂ (%)	CH ₁ (%)	CH ₂ (%)			CH ₁ (%)	CH ₂ (%)		CH ₁ (%)	CH ₁ (%)			
1	HF-1%-CH	95	0.4	49	11	28	9	91	5	1	3	9	0	0			[Dis93]
2	HF-5%-CH	25	20.0	13	69	1	8	91	5	3	1	9	0	0			[Dis93]
3	MW-Si	50	1.0	5	76	1	11	93	2	4	1	7	0	0			[Dis92]
4	MW-100-diam.	198	0.2	19	31	26	5	79	2	5	3	10	11	11			[Dis92]
5	MW-110-diam.	180	0.5	10	66	3	12	90	3	4	2	9	1	1			[Dis92]
6	MW-111-diam.	231	0.7	5	73	2	10	90	3	3	1	7	3	3			[Dis92]
7	FL-100-diam.	~17	0.4	22	10	34	1	67	19	8	6	33	0	0			[Jan92]
8	FL-110-diam.	~17	3.0	22	62	6	6	94	4	1	1	6	0	0			[Jan92]

(continued)

Table 9.3.4 (continued)

Nos.	Sample	Film thickness (μm)	Hydro-gen (at%)	aliph. sp^3		aliph. sp^3		latt. sp^3	total sp^3 (%)	olef. sp^2		arom. sp^2		Total sp^2	acetyl. sp^1	Refs.
				CH_3 (%)	CH_2 (%)	CH_1 (%)	CH_1 (%)			CH_2 (%)	CH_1 (%)	CH_1 (%)	CH_1 (%)			
9	FL-111-diam.	~ 5	1.5	23	55	2	8	88	8	3	1	12	0	[Jan92]		
10	FL-111-HT-1, 020 °C	~ 4	0.2	21	27	15	24	87	9	4	0	13	0	[Jan92]		
11	MW-0%-N ₂	11	0.9	15	74	3	2	94	2	2	2	6	0	[Dis92]		
12	MW-1%-N ₂	12	1.9	3	48	19	16	86	10	4	0	14	0	[Dis92]		
13	MW-0-Volt	ATR	-	32	28	27	12	99	0	0	1	1	0	[Joh94]		
14	MW-250-Volt	ATR	-	22	38	22	7	89	0	0	11	11	0	[Joh94]		
15	HF-as-grown	65	2.0	22	60	4	3	89	5	3	3	11	0	[Dis92]		
16	HF-HT-475 °C	65	2.0	25	15	34	17	91	2	2	5	9	0	[Dis92]		
	Average (CVD)	80	2.5	19	47	14	8	88	5	3	3	11	1	-		
17	DLC-as-grown	2	21.0	0	40	28	-	68	0	22	8	30	2	[Dis83]		
18	DLC-HT-600 °C	2	9.0	0	1	1	-	2	0	0	98	98	0	[Dis83]		
19	PAC	2	22.0	25	28	0	-	53	32	8	5	45	2	[Dis87]		

The CVD samples were prepared by microwave plasma (MW), hot filament (HF), or flame (FL)

Latt. lattice, *aliph.* aliphatic, *olef.* olefinic, *arom.* aromatic, *acetyl.* acetylenic, *diam.* diamond substrate, *ATR* attenuated total reflection, *HT* annealed at 475 °C (No. 16), 600 °C (No. 18), 1,020 °C (No. 10)

Table 9.3.5 Absorption lines from C–C bend and stretch vibrations from H-bonded carbon in diamond-related materials (RA): natural diamond coat (NDC), amorphous diamond-like carbon (DLC), and polymer-like amorphous carbon (PAC (see also Table 11.1)

Line	Assignment	NDC:H [Ang65] Energy (meV)	DLC:H [Dis87] Energy (meV)	DLC:D [Dis87] i2-shift (%)	PAC:H [Dis87] Energy (meV)	PAC:D [Dis87] i2-shift (%)
	<i>arom./olef. (sp²)</i>					
	CC bend					
	<i>aliph. (sp³) CC</i>					
	bend					
RA0104	C=C (aromatic sp ²)	104	104.1	0	104.1	0
RA0110	C–C (sp ³)	–	109.7	0	109.7	0
RA0120	C=C (olefinic sp ²)	121	120.3	–1.0	120.3	–1.0
	<i>(sp³) C–C</i>					
	stretch					
RA0144	C–C (sp ³) <i>(mixed sp²/sp³)</i>	–	143.8	0	143.8	0
	C–C stretch					
RA0154	C–C (mixed sp ² /sp ³)	–	154.4	0	154.4	0
RA0161	C–C (mixed sp ² /sp ³)	–	161.2	0	157.5	+1.2
RA0188	C–C (mixed sp ² /sp ³)	–	187.8	0	187.8	0
	<i>(sp²) C=C</i>					
	stretch					
RA0196	C=C (aromatic sp ²)	–	195.9	–1.3	195.9	–1.3
RA0201	C=C (olefinic sp ²)	–	200.8	–1.2	198.4	–1.2
	<i>(sp¹) C=C</i>					
	stretch					
RA0270	C=C (acetylenic sp ¹)	–	–	–	270.3	–
Raman	Lattice C–C (sp ³)	–	165	–	–	–

bonding lines (in the same spectral range) was achieved by a careful analysis of the spectra from deuterated samples [Dis87].

9.3.6 Additional Hydrogen Lines in Homoepitaxial CVD Diamond

In (1 0 0) epitaxial CVD diamond, two centers with correlated intensities are observed [Fuc95a],b. These lines are here tentatively assigned to $^*(V_4H_4)^\circ$.

The ZPL at 165 meV (DAP39) is typical for a C–C bond vibration. The ZPL at 412 meV (DAP40) has very small ^2H (–0.5%) and ^{13}C (–0.2%) isotope shifts. Therefore, it could be a nonvibrational transition (see Table 8.1.7.2).

9.4 Silicon in Diamond

9.4.1 Five Silicon Centers in Diamond

Optical silicon centers in diamond seem to be of limited interest, because only few respective spectra have been published (with the exception of the $^*2\text{Si}$ 1.68 center). Accordingly, Tables 8.1.6, 9.4.1, and 9.4.2 contain no more than five silicon centers. Three silicon centers occur in natural diamond ($^*2\text{Si}$ 1.68 = $(\text{V}_3\text{Si}_2)^+$, $^*\text{Si}$ 2.05 = $(\text{V}_3\text{Si}_2)^\circ$, and $^*\text{Si}$ 2.52 = $(\text{V}_3\text{Si}_2)^-$), four centers in CVD diamond, which are usually grown on Si substrates ($^*2\text{Si}$ 1.68 = $^*(\text{V}_3\text{Si}_2)^+$, $^*\text{Si}$ 2.05 = $^*(\text{V}_3\text{Si}_2)^\circ$, $^*1\text{Si}$ 2.65 = $^*(\text{V}_1\text{Si}_1)^\circ$, and $^*1\text{Si}$ 2.99 = $^*(\text{V}_1\text{Si}_1)^-$), and two centers are observed after Si ion implantation ($^*2\text{Si}$ 1.68 = $^*(\text{V}_3\text{Si}_2)^+$ and $^*\text{Si}$ 2.52 = $^*(\text{V}_3\text{Si}_2)^-$).

9.4.2 Resolved ZPL Isotope Shifts from Natural Silicon

The natural abundance of silicon isotopes is given by 92.17% (^{28}Si), 4.71% (^{29}Si), and 3.12% (^{30}Si). For two equivalent silicon atoms, the relative abundances for the five Si_2 combinations are 84.95% ($^{56}\text{Si}_2$), 8.68% ($^{57}\text{Si}_2$), 5.97% ($^{58}\text{Si}_2$), 0.29% ($^{59}\text{Si}_2$), and 0.10% ($^{60}\text{Si}_2$).

From high-quality samples, high-resolution spectra in the range 1.681–1.684 eV have been obtained, showing 12 lines [Cla95]. Experimental photoluminescence and absorption results for the $^*2\text{Si}$ 1.68 = $^*(\text{V}_3\text{Si}_2)^+$ center are given in Table 9.4.2. The agreement between calculated and observed data is excellent, both for frequencies and intensities. The isotope shift for a mass increase of one unit is –0.35 meV. From the relative intensities of the isotope shifted lines in luminescence and absorption, it is clear that two equivalent silicon isotopes are involved. Theoretically, a five-line pattern is expected, but only a three-line pattern has intensities above the detection limit of ca. 0.5% (see Table 9.4.2). It has been proposed that the three-line pattern arises from a single silicon [Cla95]; however, in this case, the lines named a57–d57 and a58–d58 in Table 9.4.2 should have roughly half the intensity of the observed values.

An elegant proof for the five-line pattern could come from a sample where the isotopes $^{59}\text{Si}_2$ and $^{60}\text{Si}_2$ are enriched, allowing the observation of the lines at 1.6807–1.6812 (see Table 9.4.2).

Table 9.4.1 Optical centers from silicon in diamond; for $(^*(V_3Si_2))^+$; see also Table 9.4.2

Defect	Observed	ZPL/L (eV)	SB-/ <i>sra</i> -DAP	D (eV)	Name/comment
Si-C interface	LA				99 meV/Si-C vibration
Si-C interface	LA				103 meV/Si-C vibration
$^*Si_1^\circ + ?$	LL	$L = 1.474$	<i>sra</i> , $\delta\alpha$ -g	+1.33	*Si 1.56/DAP lines 1.556-1.637 eV; QLYM: -46 (calc. 1Si + 2C; 47.1 meV)
$^*V_1Si_1^-$	NL, LL, ML	2.99J	113a-m	-1.33	*1Si 2.99/DAP lines 2.246-2.874 eV; Si_1 from QLYM(-74 meV, calc. 74.5) NL = Si rich nat. brown diamond (NBD) LL = Si substrate, ML = Si implanted; strain-induced line splittings and shifts
$^*V_1Si_1^\circ$	LE	2.646	109a-h (weak)	+1.49	*1Si 2.65/QLYM: +74, $w = 65$ meV/ Si_1 from QLYM/broad band at 2.86 eV
$^*V_1Si_1^\circ$	LL	2.646	110a-g (weak)	-1.49	*1Si 2.65/QLYM: -74, $w = 65$ meV/broad band at 2.45 eV
$^*(V_3Si_2)^-$	NE, NL Si impl. ME, ML	2.523	75a-j	-1.25	*2Si 2.52/QLYM: -26, -44 meV, Si_2 from QLYM (calc. 2Si = 44.9 meV)/PLE of *2Si 1.68/decay time 1.0-1.8 μs
$^*(V_3Si_2)^\circ$	NE, NL	2.052	65a-e	-1.39	*2Si 2.05/QLYM: -36, -45; LVM: -70 meV, Si_2 from QLYM (calc. 2Si = 44.9 meV)/PLE of *2Si 1.68/decay time 150-350 ns
$^*(V_3Si_2)^+$	HA, LA Si impl. MA	1.681	53a-n	1.60	*2Si 1.68/QLYM: +43; LVM: +67 meV, Si_2 from QLYM (calc. 2Si = 44.9 meV)/photochromic
$^*(V_3Si_2)^+$	HL, LL Si impl. ML	1.681	54a-g	-1.60	*2Si 1.68/QLYM: -36, -45; LVM: -65 meV/gr. st. spl. = 0.2; exc. st. spl. = 1.1 meV/ Si_2 from shifts of two equivalent Si isotopes (see Table 9.4.2)/(1 1 0) oriented dipole, decay time from 2.4 ns to 105 μs /photochromic

sra-DAP/SB-DAP = *standard*/sideband DAP with ZPL = L = limiting energy and D = dielectric factor; gr. st. spl. = ground state splitting; exc. st. spl. = excited state splitting

Table 9.4.2 Calculated and observed isotope shifts of the ${}^*2\text{Si } 1.68 = {}^*(\text{V}_3\text{Si}_2)^+$ center in diamond from natural silicon isotopes (92% ${}^{28}\text{Si}$, 5% ${}^{29}\text{Si}$, and 3% ${}^{30}\text{Si}$) in photoluminescence and absorption ($T = 10 \text{ K}$)

Line ^a	Calculated for Si_2^{b-c}			Observed [Cla95, Ste95]		
	Frequ. (eV)	Lumin. intens. (%)	Absorpt. intens. (%)	Frequ. (eV)	Lumin. intens. (%)	Absorpt. intens. (%)
a60	1.68070	0.03	0.01	–	–	–
b60	1.68090	0.04	0.04	–	–	–
a59	1.68105	0.09	0.04	–	–	–
b59	1.68125	0.13	0.12	–	–	–
a58	1.68140	1.8	0.8	1.6814	1.4(−0.4)	1.0(+0.2)
b58	1.68160	2.7	2.4	1.6816	2.9(+0.2)	2.3(−0.1)
a57	1.68175	2.7	1.2	1.6817	2.4(−0.3)	1.5(+0.3)
c60	1.68180	0.02	0.03	–	–	–
b57	1.68195	3.9	3.6	1.6819	4.8(+0.9)	3.8(+0.2)
d60	1.68200	0.01	0.02	–	–	–
a56	1.68210	26.3	10.9	1.6821	26.7(+0.4)	11.9(+1.0)
c59	1.68215	0.05	0.08	–	–	–
b56	1.68230	38.2	35.8	1.6823	38.2(±0)	34.8(−1.0)
d59	1.68235	0.02	0.06	–	–	–
c58	1.68250	1.0	1.6	1.6825	1.0(±0)	1.5(−0.1)
d58	1.68270	0.5	1.1	1.6827	0.5(±0)	1.0(−0.1)
c57	1.68285	1.4	2.3	1.6828	1.0(−0.4)	2.3(±0)
d57	1.68305	0.7	1.6	1.6831	0.5(−0.2)	1.8(+0.2)
c56	1.68320	13.6	22.9	1.6832	13.4(−0.2)	23.0(+0.1)
d56	1.68340	7.0	15.3	1.6834	6.7(−0.3)	15.3(±0)
Average difference					±0.2	±0.2

^aTwo ground states (I, II) and two excited states (III, IV) with transitions II–III (a), I–III (b), II–IV (c), and II–III (d). The label indicates the transition and the combined mass (${}^{56}\text{Si}_2$ – ${}^{60}\text{Si}_2$) of the ${}^{28}\text{Si}$, ${}^{29}\text{Si}$, and ${}^{30}\text{Si}$ isotopes, with abundances 84.95% ${}^{56}\text{Si}_2$., 8.68%: ${}^{57}\text{Si}_2$, 5.97% ${}^{58}\text{Si}_2$, 0.29% ${}^{59}\text{Si}_2$, 0.10% ${}^{60}\text{Si}_2$ (see Sect. 9.4.1.1)

^bFrequencies: The splittings in the ground and excited states are 0.2 and 1.1 meV, respectively. The isotope shift is -0.35 meV ($= -0.021\%$) per increasing mass unit (see Table 7.4)

^cIntensities for luminescence: The observed ($T = 10 \text{ K}$) relative intensities a: b: c: d = 31%: 45%: 16%: 8% are used

^dIntensities for absorption: The observed ($T = 10 \text{ K}$) relative intensities a: b: c: d = 14%: 42%: 27%: 18% are used

^eA single silicon atom can be excluded, because the calculated intensities for a30: b30: a29: b29: a28: b28: c30: d30: c29: d29: c28: d28 are (in luminescence) 0.9%: 1.4%: 1.6%: 2.2%: 28.5%: 41.4%: 0.5%: 0.2%: 0.8%: 0.4%: 14.7%: 7.4% (average difference ± 1.0), and (in absorption) 0.4%: 1.3%: 0.7%: 2.1%: 12.9%: 38.6%: 0.8%: 0.5%: 1.4%: 0.9%: 24.8%: 16.6% (average difference ± 1.2). The average difference is five times larger than for the two-silicon model; in addition, there is a general misbalance: all calculated intensities for a single ${}^{28}\text{Si}$ are larger than observed, while those for ${}^{29}\text{Si}$ and ${}^{30}\text{Si}$ are all too small

9.4.3 *Effects of Annealing*

Annealing experiments are reported for the $*2\text{Si } 1.68 = *(\text{V}_3\text{Si}_2)^+$ center. This is a very temperature stable center. A single crystal HTHP diamond was irradiated with 2 MeV electrons and subsequently annealed for 0.5 h at temperatures in the range 400–2,500 °C [Cla95]. Up to 600 °C, the intensity was unchanged. An order of magnitude increase occurs at 800 °C, followed by a fourfold decline at 1,200 °C. With further heating, the intensity gains a factor three with a maximum at 2,200 °C, followed by a considerable decline at 2,500 °C. The interpretation of this annealing behavior is difficult, because three charge states of the $*(\text{V}_3\text{Si}_2)$ center exist, and the intensities of the lines from the other charge states were not monitored in the experiment.

9.4.4 *Time-Resolved Spectroscopy*

The luminescence decay times for three of the five silicon centers in diamond have been determined (see Table 9.4.1) [Kho94]. The $*1\text{Si } 2.99$ center has a medium fast decay time (63 ns), while the $*2\text{Si } 2.52$ center is slow (1.0–1.8 μs). The $*2\text{Si } 1.68$ center has two decay times: one fast (2.4 ns) and one slow (105 μs). The latter is explained by energy transfer from a reservoir. With the present knowledge, the PLE line at 2.523 ($*2\text{Si } 2.52$ center) is a probable candidate for non-radiative decay. It should be mentioned that in time-resolved measurements, the 2.523-eV line splits up in at least six ZPLs in the range 2.523–2.572 eV, where the relative intensities depend strongly on the type of sample [Kho94].

9.4.5 *Local Vibrational Modes*

For two centers ($*2\text{Si } 2.05$ and $*\text{Si } 1.68$), LVM frequencies in the range 65–70 meV are observed (see Table 9.4.1). These are typical C–C bond vibrations near a vacancy (see Table 8.8).

9.4.6 *Quasi-Local Vibrational Modes*

For all five silicon centers, QLVM frequencies in the range 20–74 meV are observed, and they are listed in Tables 9.4.1. There is very good agreement with the corresponding calculated values (see Table 11.2).

9.4.7 *DAP Transition at Nickel Centers*

Weak DAP transitions of the sideband type are observed for all five vacancy-silicon associate centers (see Table 9.4.1). The variation in the dielectric factor D for multiple charge states is discussed in Sect. 10.6.

The DAP lines of the *Si 1.56 eV center are of the standard type, indicating a center with an unknown donor (if silicon is the acceptor).

9.4.8 Considerations for Structure Assignments

$^*(V_3Si_2)^\pm$. This proposed structure (two interstitial silicon in a triple vacancy) for the 1.681-eV center is almost certain. It is supported by four independent results:

1. The isotope shifts from natural silicon isotopes indicate *two* equivalent silicon atoms [Cla95] (see Sect. 9.4.2).
2. From polarized luminescence results, a $\langle 1\ 1\ 0 \rangle$ oriented dipole was determined;
3. The QLVM sideband indicates *two* silicon atoms (see Table 11.2).
4. Further support comes from the linear splitting into two components under $\langle 1\ 0\ 0 \rangle$ uniaxial stress [Ste94]. This is expected for a $\langle 1\ 1\ 0 \rangle$ oriented dipole.

The positive charge state is derived from the dielectric factor D of DAP53/54 (see Sects. 9.4.7 and 10.5).

$^*(V_3Si_2)^-$ and $^*(V_3Si_2)^\circ$. These centers at 2.523 and 2.052 eV provide photoluminescence excitation of the 1.681 eV $^*(V_3Si_2)^+$ center, indicating three charge states of the same structure. The DAP results (different D factors) exclude excited states of the 1.681-eV center, but provide a hint for the charge state. The QLVM sideband at 44–45 meV arises from *two* silicon atoms. Of special interest is the additional QLVM line at 26 meV from a Si_2C_8 cluster, which is expected for a (V_3Si_2) configuration, where two interstitial silicon atoms in the triple vacancy are surrounded by $(3 + 2 + 3 = 8)$ carbon atoms (see Table 11.2).

$^*V_1Si_1^-$ and $^*V_1Si_1^\circ$. The QLVM frequency of 74 meV clearly indicates a center with *one* silicon atom (see Table 11.2). From the DAP results (different D factors), the two charge states are derived (see Section and Table 10.5).

It is remarkable that in all five centers, the silicon is associated with one or three vacancies. Evidently, the large atomic radius of silicon (119 nm, compared to 76 nm for carbon, see Table 9.7.1) rules out a *substitutional* silicon center.

9.5 Nickel in Diamond

9.5.1 Twenty Nickel Centers in Diamond

At present, there are 20 centers, which are assigned to nickel in diamond (see Tables 9.5.1.1–9.5.1.2). Seven nickel centers occur in natural diamond, 17 centers in synthetic HPHT diamonds, which are grown from a nickel containing melt, and one center in CVD diamond. They are listed in Table 8.1.4 ($6Ni_1$, Ni_2 , and Ni_3 associates with a single vacancy), in Table 8.1.5 (seven interstitial Ni_1 associates with a double vacancy), in Table 8.1.6 (two interstitial Ni_2 associates with a triple vacancy), and in Tables 9.5.1.1–9.5.1.2 (the substitutional Ni_1 center and two nickel

Table 9.5.1.1 Summary of nickel centers in diamond (see also Tables 9.5.6 (anneal), 11.1 (LVLM), 11.2 (QLVM))

Nos.	ZPL (eV)	DAP lines (range) (eV)	Broad peak Abs/Lum. (eV)	EPR	DAP ^a	sta.			Name	Structure	Table	N conc. ^b	Ni impl. + ann. (lum.)	Comment
						SB (A/L)	L (eV)	D (eV)						
1	-	1.212-1.383	1.40/1.40	NE4?	16	-	1.036	1.45	*Ni-S8	$(V_2Ni)^-$	8.1.5	lo.	-	Also res. DAP (1.22 eV)
2	1.404	-	1.55/1.25	NIRIM2	-	25/26	ZPL	1.33	INI	V_1Ni^+	8.1.4	lo.	(hi.)	INI from isotope splitting
3	-	1.563-2.320	1.80/1.80	-	60	-	1.460	1.53	*Ni-S5	$(V_2Ni)N_{x+y+z}^0$	8.1.5	hi.	-	PLE of *S8
4a	1.660	-	-	-	-	-	-	-	*Ni-1.66a	$V_1Ni_2^0$	8.1.4	hi.	(lo.)	No absorption
5	-	1.678-1.821	-/1.70	-	4	-	-	1.66	*Ni-S9	$(V_2Ni)N_{x+y+z}^+$	8.1.5	hi.	-	-
6a	1.693	-	1.85/-	-	-	-	-	-	*Ni-1.69a	$V_1Ni_2^+$	8.1.4	hi.	(lo)	Line (b) at 1.940 eV
7a	1.704	-	1.82/-	-	-	83/84	ZPL	1.34	*Ni-1.70a	$V_1Ni_1^0$	8.1.4	lo.	(lo.)	-
8	-	1.808-2.620	2.19/2.19	S = 1 cc.	11	-	1.724	1.60	*INI-S7	$(V_2Ni)N_{x+y+z}^0$	8.1.5	hi.	-	INI from isotope splitting

(continued)

Table 9.5.1.1 (continued)

Nos.	ZPL (eV)	DAP lines (range) (eV)	Broad peak Abs/ Lum. (eV)	EPR	DAP ^d sta.	SB (A/L)	L (eV)	D (eV)	Name	Structure	Table	N conc. ^b	Ni impl. + ann. (lum.)	Comment
9	1.883	-	-	-	-	107/8	ZPL	1.35	*Ni 1.88a	*(V ₃ Ni ₂) ^o	8.1.6	hi.	-	Lines (b, c) at 1.906/ 1.913 eV
6c	1.991	-	2.16/1.85	-	-	-/111	ZPL	1.34	*Ni 1.69c	*V ₁ Ni ₂ ⁺	8.1.4	hi.	lo.	
10a	2.071	-	-	-	-	-/87	ZPL	1.34	*Ni 2.07a	*V ₁ Ni ₂ ⁻	8.1.4	hi.	hi.	No absorp- tion Table 9.5.3
11	2.157	-	-	-	-	-	-	-	*Ni 2.16	?	9.5.1.2	hi.	hi.	Table 9.5.3
12	2.267	-	-	-	-	-	-	-	*Ni 2.27	?	9.5.1.2	hi.	-	Table 9.5.3-
10b	2.298	-	2.48/	-	-	27/28	ZPL	1.34	*Ni 2.07b	*V ₁ Ni ₂ ⁻	8.1.4	hi.	hi.	PLE of *Ni 2.07a
13	2.370	-	-/2.20	-	-	91/92	ZPL	1.34	*Ni 2.37	*V ₁ Ni ₃ ^o	8.1.4	hi.	lo.	"A" line, Ni ₃ from QLVM
14	-	2.496- 2.890	2.85/2.85	NE1	58	-	2.383	1.63	Ni- S3	(V ₂ Ni ₁)Ni ₂ +0+0 ⁺	8.1.5	hi.	lo.	-

7b	2.401	-	2.63/-	-	29/-	ZPL	1.34	*Ni 1.70b	$V_1Ni_1^{\circ}$	8.1.4	lo.	lo.	PLE of *Ni 1.70a
15	-	2.515- 3.341	2.79/2.79	NE2	57	2.422	1.63	Ni-S2	$(V_2Ni_1)N_{2+0+1}^+$	8.1.6	High	hi.	"B-E" lines
4b	2.427	-	-	-	-	-	-	*N 1.66b	* $V_1Ni_2^{\circ}$	8.1.4	hi.	lo.	PLE of *Ni 1.66a
16	2.510	-	-	W8	-	-	-	Ni 2.51	Ni_1^-	9.5.1.2	hi.	lo.	T_d symmetry
17a	2.562	-	-/2.35	-	105/6	ZPL	1.55	*2Ni 2.56a	* $(V_3Ni_2)^+$	8.1.6	lo.	hi.	2Ni from isotope splitting
18	-	2.750- 3.530	3.00/300	NE8?	61	2.637	1.63	*Ni- S6	* $(V_2Ni_1)N_{x+y+z}^+$	8.1.5	hi.	-	PLE of *S5, *S8
17c	3.065	-	3.54/-	-	-	-	-	*2Ni 2.56c	* $(V_3Ni_2)^+$	8.1.6	lo.	(hi.)	Lines (b, d) at 2.588, 3.076eV
19	-	3.333- 3.820	3.30/3.30	NE3	59	3.191	1.53	Ni-*S4	$(V_2Ni_1)N_{1+2+0}^{\circ}$	8.1.8	hi.	-	PLE of S2, *S8

^aL = limiting energy, D = dielectric factor

^bN conc.: lo. = ca. 5-10 ppm, hi. = ca. 250 ppm. References [Law93a, Kup99, Col00, Zai01]

Table 9.5.1.2 Additional data on nickel centers in diamond

Nos.	ZPL (eV)	Structure	Observed	Name	Comment
16	2.510	*Ni ₁ ⁻	HA, MA, HL, ML <i>EPR:W8</i>	*Ni 2.51(a)	T _d symmetry/3 components at 4 K: 2.509, 2.510, 2.511 eV/correlates with W8 EPR center of Ni ₁ ⁻ (3d ⁷ , S = 3/2)
16	2.523	*Ni ₁ ⁻	HA,MA, HL,ML	*Ni 2.51(b)	Line (b) is three times weaker than line (a)
20	2.436	*(C ₂) _i Ni ₁ ^o	ML	*Ni 2.44	Resonance/SB DAP14(2.066– 2.271 eV), resonance lines at 2.156 (V ₁ Ni ₁ ^o) and 2.427 eV (V ₁ Ni ₂ ⁺ (b)); QLVM: –75 meV
11	2.157	Ni+?	ML	*Ni 2.16	Ni implanted +1, 400 °C annealing; QLVM: –40 meV (calc. 38.9 meV for 1Ni + 1C)
12	2.267	Ni+?	HA,MA, HL,ML	*Ni 2.27	QLVM: +49 meV (calc. 49.7 meV for 4C)

centers with unknown structure). It is remarkable that at least 15 of the 20 nickel centers are nickel-vacancy associates, which is probably due to the large ionic radius of nickel.

For three centers, the involvement of nickel is evident from resolved splitting due to nickel isotopes (Sect. 9.5.2). Direct evidence for nickel involvement is obtained for ten centers, which are produced by nickel implantation (Sect. 9.5.3). Further arguments for the assignment to nickel come from the observation of related EPR centers (Sect. 9.5.4).

Only for three nickel centers, the structure is confirmed by EPR (S2, S3, and *S4; see Tables 8.1.5 and 9.5.1.1). For 13 additional centers, the proposed structure (marked by a preceding *) is based on information from characteristic LVM frequencies (Sect. 9.5.7 and Table 9.5.7), from QLVM frequencies (Sect. 9.5.8 and Table 9.5.8), and from DAP transition analysis (Sect. 9.5.9).

In Table 9.5.1.2 additional data for the nickel centers Nos. 11, 12, 16, and 20 are given. For two nickel centers (nos. 11, 12) the structure is unknown. The substitutional single nickel center (no. 16 = *Ni₁⁻) correlates with the W8 EPR center. The associate of nickel with the carbon split self interstitial (no. 20 = *(C₂)_iNi₁^o) is not contained in Tables 9.5.1.1 and 9.5.6.

9.5.2 Resolved Isotope Shifts from Natural Nickel

The natural abundance for *one* nickel atom (odd mass in *italics*) is given by 67.77% (^{58}Ni), 26.16% (^{60}Ni), 1.25% (^{61}Ni), 3.66% (^{62}Ni), and 1.16% (^{64}Ni).

For *two* equivalent nickel atoms, the relative abundances for the 11 Ni_2 combinations (odd masses in *italics*) are 45.93% ($^{116}\text{Ni}_2$), 35.46% ($^{118}\text{Ni}_2$), 1.15% ($^{119}\text{Ni}_2$), 11.80% ($^{120}\text{Ni}_2$), 0.65% ($^{121}\text{Ni}_2$), 3.50% ($^{122}\text{Ni}_2$), 0.09% ($^{123}\text{Ni}_2$), 0.74% ($^{124}\text{Ni}_2$), 0.03% ($^{125}\text{Ni}_2$), 0.08% ($^{126}\text{Ni}_2$), and 0.01% ($^{128}\text{Ni}_2$).

Experimental results for three nickel centers are given below and in Table 7.5. The isotope splitting for zero phonon lines is small (0.16–1.60 meV) and is resolved only in favorable cases. Surprisingly large (8–13 meV) is the splitting for the five DAP transitions of *S7 (see Table 7.5).

(2) ***1Ni 1.40 center** = $^*\text{V}_1\text{Ni}_1^+$: Four resolved isotope-shifted lines from a single nickel atom are observed, with a separation of +0.16 meV (decreasing mass) for the even isotopes. A separation of +0.22 meV is estimated for the not well-resolved isotope ^{61}Ni [Dav89]. For decreasing energy, the relative intensities (*uneven isotope in italics*) are 72%: 21%: 1.4%: 4.2%: 1.4%. This is in good agreement with the natural Ni_1 isotope abundance.

(8) ***Ni-S7** = $^*(\text{V}_2\text{Ni}_1)\text{N}_{x+y+z}^+$ at 1.80–2.62 eV: Nickel isotope shifts with three resolved components are observed on the five DAP11 transitions with $s = 9, 14, 22, 64,$ and 162 . The separation varies between +8 and +12 meV for increasing mass (^{58}Ni , ^{60}Ni , and ^{62}Ni). The relative intensities agree with the natural abundances of a single nickel atom, as demonstrated by simulated spectra [Iak00g].

(17a) ***2Ni 2.56 center** = $^*(\text{V}_3\text{Ni}_2)^+(\text{a})$: Five groups of isotope-shifted luminescence lines are observed with a separation of +1.6 meV (for decreasing mass), denoted by I (2.558 eV)–V (2.564 eV). The exact separation is 1.60 ± 0.05 meV for I–II–III, 1.56 ± 0.05 meV for III–IV, and 1.49 ± 0.05 meV for IV–V. Each group consists of three components (denoted a,b,c) with a separation of 0.37 meV for a–b, and 0.30 meV for b–c [Col83b, Col90c, Col97]. From the temperature dependence of the spectra, it is evident that the 1.49–1.60 meV splitting I–V (isotope shift) occurs in the excited state, and the 0.30–0.37 meV splitting a–c occurs in the ground state. The relative intensities of the components a:b:c at the temperature 16 K are (I) 1%: 3%: 0%, (II) 16%: 21%: 0%, (III) 4%: 12%: 0%, (IV) 0%: 8%: 4%, and (V) 0%: 0.2%: 1%.

Unfortunately, the relative intensities of I–V do not allow a straightforward analysis for three reasons:

1. The luminescence decay time varies drastically from 10.5 ns at 77 K over 0.8 ms at 20 K to 140 μs at 2.3 K, indicating interaction with a reservoir;
2. Thermal depopulation of the higher states in the excited state starts below 88 K (begin of resolved structure) and is very pronounced down to 1.8 K;
3. The relative intensities of some lines are not reproducible (the spectrum at 4.2 K is very different from the spectra at other temperatures). This is a hint for partial absorption inside the crystal (see below).

To eliminate the influence of depopulation, Boltzmann statistics can be applied. For the present analysis, depopulation-corrected intensities have been calculated. The result for the 16 K spectrum is 0.12: 3.5: 4.6: 12.4: 4.3 (for calibration, see below).

A more serious difficulty is the loss of intensity by self-absorption. This loss is different for the groups I–V. Since the loss of group II is the smallest, this group can be used for a pseudo-calibration (0% loss assumed), i.e., the intensity of group II is given the theoretical value of 3.5% (see above). By comparison with the theoretical intensities, the relative absorption losses (at 16 K) can be obtained, and are 80% (I), 60% (III), 65% (IV), and 90% (V). Depth-dependant luminescence spectra are desirable.

In spite of this unsatisfactory situation, the involvement of two equivalent nickel atoms can be concluded from the *five* equidistant groups I–V (a single nickel atom can account only for *four* equidistant groups). In addition, there is great similarity to the well-understood corresponding silicon center $^*(V_3Si_2)^+$ at 1.681 eV (see Sect. 9.4). This silicon center has a 0.22-meV splitting in the ground state and +0.35-meV isotope splitting (for decreasing mass) in two excited states (with 1.1 meV separation). For the corresponding nickel center, a similar second excited state ($^*(V_3Ni_2)^o(b)$ at 2.588 eV) is observed, with a spectral separation of 24 meV and an activation energy of 23.8 eV [Col83b].

In absorption and photoluminescence excitation, two further excited states ($^*(V_3Ni_2)^+(c,d)$) are observed at 3.065 and 3.076 (see Table 8.1.6). The weak structure on the 3.065 eV line may arise from isotope splitting.

9.5.3 Nickel Implantation and Resulting Centers

A natural type IIa diamond (containing nitrogen) has been implanted with 340 keV Ni^+ ions at a dose of 10^{14} cm^{-2} , and subsequently annealed at 1,400 °C [Zai00a]. The published CL spectrum is restricted to the energy range 1.95–2.70 eV. The following ten nickel centers are observed (intense lines are underlined): *Ni 1.69(c) at 1.991 eV; *Ni 2.1(a) from $^*V_1Ni_2^-$ at 2.071 and (b) at 2.298 eV; *Ni 2.16 at 2.157 eV; *Ni 2.37 from $^*V_1Ni_3^o$ at 2.370 eV; *Ni 1.70(b) from $^*V_1Ni_1^o$ at 2.401 eV; *Ni 1.66(b) from $^*V_1Ni_2^+$ at 2.427 eV; *Ni 2.51 from Ni_1^- at 2.510 eV; Ni-S2 from $(V_2Ni_1)N_{2+0+1}^+$ with lines B at 2.537, C at 2.597, and D at 2.623 eV; *2Ni 2.56 from $^*(V_3Ni_2)^+$ at 2.562 eV; and Ni-S3 from $(V_2Ni_1)N_{2+0+0}^+$ at 2.653 eV.

Additional lines (not related to nickel) are observed from $V_1Ni_1^o$ (NV center) at 2.154 eV, from $V_1N_2^o$ (H3 center) at 2.464 eV, and from $V_2N_4^o$ (H4 center) at 2.497 eV. Also observed are 14 lines from DAP1 transitions (nitrogen + boron pair) in the range 2.070–2.649 eV.

In a previous experiment (nickel implantation and 1,400 °C annealing), it had been found that the *1Ni 1.40 center (from $^*V_1Ni_1^+$) and the *2Ni 2.56 center (see above) arise from nickel [Gip83].

9.5.4 *Electron Paramagnetic Resonance and Zeeman Effect of Nickel Centers*

The most important EPR centers are *NE1*, *NE2*, and *NE3* with their optical counterparts *S3*, *S2*, and **S4*. Note, that the *NE3* EPR center is in the positive state, while the optical counterpart **S4* is in the neutral charge state. Evidently the two charge states coexist. The complicated structure of these centers was derived from the analysis of the hyperfine interaction [Nad93]. The interstitial nickel atom resides midway between two adjacent lattice vacancies. Different numbers of nitrogen atoms are found in the first, second, and third shell around the nickel atom. In the unrelaxed lattice, the distance to these sites (relative to the diamond lattice bond r_0) are $r_1 = 1.26 r_0$, $r_2 = 1.82 r_0$, and $r_3 = 2.06 r_0$. The average hyperfine interaction is $A_1 = 15.5$, $A_2 = 5.6$, and $A_3 = 2.6$ Gauss. This is in good agreement with the ratio $1/r^3$ of the three shells, which is 15.5: 5.3: 3.4. Counting the number of nitrogen atoms in the three shells leads to the notation $S2 = (V_2Ni_1)N_{2+0+1}$, $S3 = (V_2Ni_1)N_{2+0+0}$, and $*S4 = (V_2Ni_1)N_{1+2+0}$ (see also Sects. 8.1.5 and 9.5.3).

The **W8** EPR center arises from Ni_1^- ($3d^7$) with an effective spin of 3/2 and is assigned to the optical 2.510 eV center (substitutional Ni_1 with T_d symmetry) [Col00].

The **NIRIM 2** EPR center has been assigned to the optical 1.40 eV center [Iso90a].

The $1Ni^*S7$ center at 1.808–2.620 eV (observed only in CVD samples) is closely related to the $S = 1$ EPR center [Iak00a].

Four EPR Ni centers without a confirmed optical counterpart are **NE4**, **NE5**, **NE8**, and **NIRIM 1** [Col00].

9.5.5 *Influence of Nitrogen Concentration*

It is a remarkable property of the nickel centers that 14 of them occur (more or less exclusively) in diamond with *high* nitrogen concentration, and only four centers in diamond with *low* nitrogen concentration. The latter are $*(V_2Ni_1)^-$, $*V_1Ni_1^+$, $*V_1Ni_1^0$, and $*(V_3Ni_2)^-$ (see Tables 9.5.1.1 and 9.5.6).

In the present structure assignment, only the seven centers $S2$ – $*S7$, $*S9$ contain nitrogen. The centers $V_1Ni_2^-$, $V_1Ni_2^0$, $V_1Ni_2^+$, and $V_1Ni_3^0$ might contain nitrogen. Experiments with the search for ^{15}N isotope shifts are desirable.

9.5.6 *Effects of Annealing of Nickel Centers*

The annealing effects and thermal stability of nickel centers in diamond are summarized in Table 9.5.6. Fourteen nickel centers are observed in as-grown HPHT diamonds (nos. 3–5, 14 are missing in low temperature-grown HPHT diamonds

Table 9.5.6 Observed annealing effects and thermal stability of nickel centers in diamond (see also Table 9.5.1.1)

No	ZPL (eV)	DAP lines (range) (eV)	Name	Structure	N conc. ^d	Before anneal		Anneals out at	Anneals out at	Text in [Zai01] page	Comment temperatures in °C
						Natural	HPHT				
1	-	1.212–1.383	*S8	$*(V_2Ni_1)^-$	lo.	-	HA, HL	-	>1,800	134	Photochromic at < 1.7 eV
2	1.404	-	1Ni 1.40	$*V_1Ni_1^+$	lo.(hi.)	NA, NL	HA, HL	>1,800	>2,500	140	C_{3v} symmetry, photochromic at > 1.7 eV
3	-	1.563–2.320	*S5	$*(V_2Ni_1)^0$ N_{x+y+z}^0	hi.	NA, NL	HA, HL	>1,800	>1,800	148	Strengthened at $T > 1,500$
4a	1.660	-	*Ni 1.66a	$*V_1Ni_2^0$	hi.	-	-	-	<2,200	156	ML appears after $T > 1,500$; no abs.
5	-	1.678–1.821	*S9	$*(V_2Ni_1)^+$ N_{x+y+z}^+	hi.	-	-	-	-	183	ML appears after N irradiation. $T = 950$
6a	1.693	-	*Ni 1.69a	$*V_1Ni_2^+$	hi.	-	HA, HL	<1,800	<1,800	182	Strengthened at 1,500 < T < 1,800
7a	1.704	-	*Ni 1.70a	$*V_1Ni_1^0$	lo.	-	HA, HL	<1,800	<1,800	183	

8	-	1.808— 2.620	*S7	* $(V_2Ni_1)^+$ N_{x+y+z}	hi.	-	-	>1,800	?	-	Only in CVD samples [Iak00a]
9	1.883	-	*Ni 1.88a	* $(V_3Ni_2)^{\circ}$	hi.(lo.)	-	HA, HL	<1,800	-	192	Transforms into * $V_1Ni_2^+$
6c	1.991	-	*Ni 1.69c	* $V_1Ni_2^+$	hi.	-	HA, HL	>1,800	<2,200	197	Strengthened at $T > 1,500$; line (b) at 1,940
10a	2.071	-	*Ni 2.07a	* $V_1Ni_2^-$	hi.	-	-	>1,800	<2,200	209	Appears after $T > 1,500$; No absorption
11	2.157	-	*Ni 2.16	?	hi.	-	-	-	>1,800	226	Appears after $T > 1,700$
12	2.267	-	*Ni 2.27	?	hi.	-	HA, HL	-	>1,800	234	Strengthened at $T > 1,500$
10b	2.298	-	*Ni 2.07b	* $V_1Ni_2^-$	hi.	-	-	>1,800	<2,200	236	Appears after $T > 1,500$
13	2.370	-	*Ni 2.37	* $V_1Ni_3^{\circ}$	hi.	NA, NL	-	-	>1,800	248	"A" line
14	-	2.496— 2.890	S3	$(V_2Ni_1)^+$ N_{2+0+0}^+	hi.	NA, NL	HA, HL	>1,800	>1,800	277	Inactive in CL

(continued)

Table 9.5.6 (continued)

No	ZPL (eV)	DAP lines (range) (eV)	Name	Structure	N conc. ^a	Before anneal		Anneals out at 1,400–1,800 °C	Anneals out at 2,000–2,500 °C	Text in [Zait01] page	Comment temperatures in °C
						Natural	HPHT				
7b	2.401	–	*Ni 1.70b	$V_1Ni_1^{\circ}$	lo.	–	HA	–	< 2,200	255	PLE of *Ni 1.70a
15	–	2.515–3.341	S2	$(V_2Ni_1) N_{2+0+1}^{+}$	hi.	NA, NL	HA, HL	> 1,800	> 1,800	287	*B–E* lines, inactive in CL
4b	2.427	–	*N 1.66b	$*V_1Ni_2^{\circ}$	hi.	–	HA, HL	> 1,800	< 2,200	256	PLE of *Ni 1.66a, strengthened at $T > 1,500$
16	2.510	–	*Ni 2.51	$*Ni_1^{-}$	hi.(lo.)	–	HA, HL	< 1,600	–	283	Line (b) at 2.588 eV
17a	2.562	–	*2Ni 2.56a	$* (V_3Ni_2)^{+}$	lo.	NA, NL	HL	> 1,800	> 1,800	290	Appears after $T > 2,200$, PLE of *S5
18	–	2.750–3.530	*S6	$* (V_2Ni_1) N_{x+y+z}^{+}$	hi.	–	–	> 1,800	> 1,800	303	PLE of 2Ni 2.56a,b, line (d) at 3.076 eV
17c	3.064	–	*2Ni 2.56c	$* (V_3Ni_2)^{+}$	lo.	NA/NE	HA/HE	> 1,800	> 1,800	324	PLE of S2, *S8
19	–	3.333–3.820	*S4	$* (V_2Ni_1) N_{1+2+0}^{\circ}$	hi.	NA/NE	HA/HE	–	> 1,800	334	

^aN concentration: lo. = ca. 5–10 ppm, hi. = ca. 250 ppm [Law93a, Kup99, Col00, Zait01]

[Law93a]), three centers (nos. 9, 10, 17; all with high nitrogen concentration) appear after annealing at 1,500–2,500 °C, and one center (no. 7) exists only in CVD diamond.

In diamonds with high nitrogen concentration, substantial changes in the nickel spectra occur in the temperature range 1,500–1,900 °C. This is the temperature regime where single substitutional nitrogen is transformed into aggregated structures (see Sect. 9.1.6.1). In parallel with the nickel spectra, the infrared absorption of nitrogen centers was monitored with the following result: *as grown*: 100 ppm N_1 (C-center) + 6 ppm N_2 (A center); *after 1,600 °C anneal*: 37 ppm N_1 + 82 ppm N_2 ; *after 1,800 °C anneal*: 4 ppm N_1 + 115 ppm N_2 [Law93a]. These infrared spectra also show intense absorption from the N_1^+ (X center, lines at 165, 130, and 118 meV (or 1,332; 1,046; and 950 cm^{-1}); see Table 9.1.2), which is preferentially observed in nickel-containing diamonds, and anneals out at 1,900 °C. This absorption is proportional to the concentration of compensated boron [Zai01].

In contrast to the nitrogen-rich samples, the nickel spectra in diamonds with low nitrogen concentration show almost no annealing effects, except for a general weakening of the signals at 1,800 °C [Law93a].

The influence of nitrogen aggregation on the annealing behavior of nickel centers in diamond with high nitrogen concentration is quite evident. After the nitrogen aggregation, a shift in the Fermi level toward the valence band is expected, with a corresponding change in charge state of the nickel centers. This effect cannot be further discussed because the charge state for most of the nickel centers is not yet confirmed.

Alternatively, a change in structure can occur when vacancies in nickel-vacancy associates recombine with migrating carbon interstitials (see (9.2b) and (9.3b)). A direct proof for this annealing effect (at $T < 1,800$ °C) is given by the quantitative transformation of $^*(V_3Ni_2)^\circ$ at 1.883 eV into $^*V_1Ni_2^+$ at 1.693 eV [Law93a].

A further possibility is the partial dissociation of nickel associates. Of interest is also the appearance of the DAP1 absorption transitions. Some ten lines (1.938–2.648 eV) arise from this center, which is free of nickel, and has been assigned to the $N_1^\circ + B_1^\circ$ pair (see Sect. 9.1.5 [Dis94a],b). In the samples with high nitrogen concentration, these lines appear after 1,500 °C annealing. After a 1,800–2,200 °C annealing, only the close pairs in shells 1–3 are present, while all distant pairs have disappeared (by dissociation) [Law93a, Kup99].

The thermal stability of the nickel centers has been investigated in the temperature range 1,600–1,900 [Law93a] and 2,200–2,500 °C [Kup99]. The results are listed in Table 9.5.6. All seven nickel centers, which occur in natural diamond, are stable at least up to 2,200 °C.

9.5.7 Local Vibrational Modes

LVM frequencies for nickel centers in diamond are listed in Tables 2.1.1.1–5.4.4. There is good agreement between the predicted and observed LVM frequencies, which supports the present structure assignments (see Table 9.5.7).

Table 9.5.7 Predicted and observed LVM frequencies of nickel centers in diamond

	Table Defect	Observed LVM frequencies (meV)				
		8.1.4 V_1Ni_1	8.1.4 V_1Ni_2	8.1.4 V_1Ni_3	8.1.4 $(V_2Ni_1)N_n$	8.1.6 (V_3Ni_2)
Type of vibration	Predicted ^a					
Ni(sp ³) – –C/N(sp ³) bend	27–45 ^b	–	–	–	–	–
C/N(sp ³) – –C (sp ³) bend	45–75 ^c	61	49–61 (1x–7x) ^d	49	–	–
Ni(sp ³) – –Ni(sp ³) stretch	45–81 ^e	–	–	–	–	61–65
Ni(sp ³) – –C/N(sp ³) stretch	58–106 ^b	74–80	64–66	70	63–99	–
C/N(sp ³) – –C (sp ³) stretch	97–177 ^c	100–127	–	–	102–144	–

^aThe predicted values are obtained from data in Table 8.8 by multiplication (for the heavier mass of ⁵⁹Ni) with the appropriate factor

^bFactor 0.60

^cFactor 1.0

^dNumber of harmonics

^eFactor 0.46

9.5.8 Quasi-Local Vibrational Modes

Valuable information on the structure of nickel centers is obtained from the QLVM sidebands, as shown in Table 9.5.8. This table is subdivided in QLVM frequencies of 3 Ni (23 meV), 2 Ni (25–30 meV), and 1 Ni (29–46 meV).

9.5.9 DAP Transition at Nickel Centers

With three exceptions (nos. 10, 11, and 15 in Tables 9.5.1.1 and 9.5.1.2), all nickel centers are associates with one, two, or three lattice vacancies. In principle, DAP transitions from all these centers should exist, and indeed for only two (nos. 4 and 5), the DAP lines are not yet observed. A special case is that of *standard* DAPs of the centers S2 to *S9, where the interstitial nickel resides midway between two vacancies. The nickel d electrons form bonds with the six equidistant carbon neighbors, thus avoiding dangling bonds, which would produce a *sideband* DAP. For the centers S2 to *S9 the dielectric factor D depends on the charge state, and is 1.60–1.66 eV for S2⁺, S3⁺, *S6⁺, *S7⁺, *S9⁺, is 1.53 eV for *S4^o, *S5^o, and

Table 9.5.8 Calculated and observed QLVM frequencies of Ni centers

Atoms	Calculated ^a (meV)		Observed (meV)		ZPL/or <i>L</i> ^b	Center	Tables
	Frequ.	Width	Frequ.	Width	(eV)		
3 Ni	23.3	5.8	-23	10	2.370	*V ₁ Ni ₃ ^o	8.1.4
2 Ni + 2C	26.2	7.3	-25	8	2.562	*(V ₃ Ni ₂) ^o (a)	8.1.6
			+26	7	3.064	*(V ₃ Ni ₂) ^o (b) = 2.562(b)	8.1.6
2 Ni	29.0	9.0	-26	10	1.883	*(V ₃ Ni ₂) ⁺	8.1.6
			+30	11	2.298	*V ₁ Ni ₂ ^o (b) = 2.071(b)	8.1.4
			+28	12	2.427	*V ₁ Ni ₂ ⁺ (b) = 1.660(b)	8.1.4
1 Ni + 2N + 2C	30.0	9.5	+29		2.422	S2 = (V ₂ Ni ₁)N ₂₊₀₊₁ ⁺	8.1.5
			+30		2.383	S3 = (V ₂ Ni ₁)N ₂₊₀₊₀ ⁺	8.1.5
1 Ni + 1N + 3C	30.3	9.7	-31		3.191	* S4 = (V ₂ Ni ₁)N ₁₊₂₊₀ ⁺	8.1.5
			-33		1.460	* S5 = (V ₂ Ni ₁)N _{1+x+y} ^o	8.1.5
1 Ni + 3C	32.8	11.4	-32	12	2.071	*V ₁ Ni ₂ ^o (a)	8.1.4
1 Ni + 2N	34.5	12.6	+34		2.422	S2 = (V ₂ Ni ₁)N ₂₊₀₊₁ ⁺	8.1.5
1 Ni + 2C	35.5	13.3	+34	11	2.401	*V ₁ Ni ₁ ^o (b)= 1.704(b)	8.1.4
			-36	15	2.562	*(V ₃ Ni ₂) ^o (a)	8.1.6
1 Ni + 1C	38.9	16.1	-40	18	2.157	*Ni ₁ + X	9.5.1.2
1 Ni	43.6	20.2	+42		1.460	* S5 = (V ₂ Ni ₁)N _{1+x+y} ^o	8.1.5
			+42		2.637	* S6 = (V ₂ Ni ₁)N _{2+x+y} ⁺	8.1.5
			-44	20	1.704	*V ₁ Ni ₁ ^o (a)	8.1.4
			+45	25	1.404	*V ₁ Ni ₁ ⁺	8.1.4
			-46		2.422	S2 = (V ₂ Ni ₁)N ₂₊₀₊₁ ⁺	8.1.5

^aSee Table A.3

^b*L* = limiting energy for standard DAPs (no ZPL)

is 1.45 eV for *S8⁻ (see Sect. 10.5). Since the vacancy is the dominant defect in nickel-vacancy associates, the corresponding DAP spectra are already discussed in Sect. 8.3.2.

A decisive help in the analysis of DAP16 (*S8 = *(V₂Ni₁)⁻) is the simultaneous appearance of resonance DAP lines from this center in some samples [Law93c]. The 12 lines peak at 1.22 eV and allow the determination of the parameters *L* and *D* for this DAP, which in most samples produces only an unstructured broad band, peaking at 1.40 eV.

9.5.10 *The S2 to *S9 Family (DAP57–61, 11, 16, 4) with the (V₂Ni₁) Nucleus and 0–3 Nitrogen Ligands*

The almost 100 lines of the S2 to *S9 family have never been really explained until this book was written. The observation of coinciding energies for absorption and luminescence is very intriguing, and an explanation by zero phonon lines was generally assumed [Zai01]. The present DAP interpretation (see Tables 8.1.9, 9.5.10 and 10.1) can satisfactorily explain the line positions and the coincidence of absorption and luminescence. The latter is characteristic for *standard* DAPs (see Sect. 10.1).

By the pioneering work of [Yel92a],b and [Nad93], the structure of three optical centers was determined from their EPR counterpart. These are **S2** with EPR center NE2, **S3** with EPR center NE1, and ***S4** (sometimes named “523 nm” center) with EPR center NE3. (It turned later out that the 523 nm = 2.370 eV line “A” is not part of the *S4/NE3 center, but is the ZPL transition of DAP91/92 = V₁N₃[◦] with a very effective energy transfer from *S4 to V₁N₃[◦]). For this book, the names *S5 to *S9 are introduced for centers with very similar structure (see Tables 8.1.9 and 9.5.6).

The S2 to *S9 family provides interesting insight into the mechanism of DAP transitions. From Table 9.5.10, it is evident that both *intra-center* DAP pairs (shell numbers 1 and 2) and distant pairs are observed. For *S8 (with zero nitrogen) only distant pairs are observed. This observation indicates that in the *intra-center* pairs (shell numbers 1 and 2 of S2, *S5, *S6, and *S7), the nitrogen ligands act as donor, and the nickel nucleus acts as acceptor.

9.5.11 *Discussion of 20 Individual Nickel Centers*

In the past, only four structure assignments have been made: S2, S3, *S4, and *Ni₁⁻. The present structure assignments for 12 additional centers are based on a combination of arguments.

The QLVM frequencies indicate the number of Nickel atoms in the center (see Sect. 9.5.8 and Table 9.5.8).

A further hint is obtained from the LVM frequencies (see Tables 8.1.4, 8.2.3, and 9.5.7). Characteristic for the V₁Ni₂ centers is the bonding vibrations with frequencies of 49–57 meV with up to six harmonics.

The 20 nickel centers are discussed in order in Tables 9.5.1.1, 9.5.1.2, and 9.5.6:

1. ***(V₁Ni₁)⁻** = Ni-S8-DAP16a-l (1.212–1.383 eV): This is the only center of the S2 to *S9 family with *no* nitrogen ligands. It is observed in diamonds with low nitrogen concentration (e.g., grown with nitrogen getter). The DAP16 transitions are of the *resonance* type (see Chap. 10) with neighboring shell numbers: 42, 43, 44, and 47, 48, 49, 50, 51. Possibly, the EPR counterpart is the paramagnetic NE4 center.
2. ***V₁Ni₁⁺** = 1Ni 1.40 at 1.401 and 1.404 eV with DAP25a-k (1.485–2.070 eV) in absorption, and DAP26a-k (1.000–1.333 eV) in luminescence.

Table 9.5.10 Survey of the DAP analysis of the S2 to *S9 family

Shell no. ^a	S2	S3	S4	S5	S6	S7	S8	S9	Comment	Name	Dielectric factor	Limiting energy, <i>L</i> (eV)	Structure
228	a	a	-	-	-	a	-	-		S2	+1.63	2.422	(V ₂ Ni ₁) N ₂₊₀₊₁ ⁺
162	b	b	-	a	a	b	-	-	S2: line B	DAP57			
98	c	-	-	-	-	-	-	-		S3	+1.63	2.383	(V ₂ Ni ₁) N ₂₊₀₊₀ ⁺
86	-	-	a	b	-	-	-	-		DAP58			
72	d	-	-	-	-	-	-	a		*S4	+1.53	3.191	(V ₂ Ni ₁) N ₁₊₂₊₀ ^o
64	e	-	-	-	-	c	-	b	S2: line C	DAP59			
58	-	-	-	c	-	-	-	d	S9: c = 62	*S5	+1.53	1.460	*(V ₂ Ni ₁) N _{3+y+z} ^o
50	f	c	b	d	-	-	b	g	S8: a = 51	DAP60			
48	g	-	-	-	-	-	d	-	S8: c = 49	*S6	+1.63	2.637	*(V ₂ Ni ₁) N _{3+y+z} ⁺
44	h	d	-	-	-	-	f	-	S8: e = 47	DAP61			
42	-	e	-	-	-	-	h	h	S8: g = 43	*S7	+1.60	1.724	*(V ₂ Ni ₁) N _{3+y+z} ⁺
38	i	-	-	-	-	-	-	-		DAP11			
34	j	f	c	-	-	d	-	-		*S8	+1.45	1.036	*(V ₂ Ni ₁) ⁻
32	k	-	-	-	-	-	-	-		DAP16			
30	l	-	-	e	-	-	-	-		*S9	+1.66	1.509	*(V ₂ Ni ₁) N _{3+y+z} ⁺

(continued)

Table 9.5.10 (continued)

Shell no. ^a	S2	S3	S4	S5	S6	S7	S8	S9	Comment	Name	Dielectric factor	Limiting energy, L (eV)	Structure
26	m	g	d	-	-	-	i	-					
22	n	-	e	-	b	e	-	i					
18	-	-	f	-	-	-	j	-					
16	-	-	-	-	c	f	-	-					
14	-	-	g	-	d	g	k	-					
13	-	-	-	-	-	-	l	-					
12	-	h	h	-	e	-	-	-					
10	-	i	i	-	-	-	-	-					
9	-	-	-	-	f	h	-	-					
8	-	j	j	f	g	-	-	-					
7	-	-	-	g	h	-	-	-					
6	-	-	k	h	i	i	-	-					
5	-	-	-	-	j	j	-	-					
4	-	-	l	i	k	k	-	-					
3	-	-	-	-	-	l	-	-					
2	o	-	-	j	l	m	-	-					
1	p	-	-	k	m	n	-	-					

^aHigh abundance shells in bold type (see Table A.2)

The involvement of a single nickel atom is evident from the resolved isotope shifts (see Table 7.5 and Sect. 9.5.2). The center is a typical vacancy associate (see Table 8.1.4). The charge state is derived from the EPR counterpart NIRIM2.

3. $^*(\mathbf{V}_2\mathbf{Ni}_1)\mathbf{N}_{x+y+z}^\circ =^*$ Ni-S5-DAP60a-k (1.563–2.320 eV). This is a typical member of the S2 to $^*\text{S9}$ family (see Sect. 9.5.3 and Table 9.5.6). For the number of nitrogen atoms in the first shell, see Sect. 9.5.2.9. The neutral charge state is assigned according to Sect. 10.5.
4. **(a,b)** $^*\mathbf{V}_1\mathbf{Ni}_2^\circ =^*$ Ni 1.66a,b at (a) 1.660 and (b) 2.427 eV. This center is absent in as-grown synthetic or natural diamonds, but appears after heat treatment ($T > 1,500^\circ\text{C}$). The Ni_2 structure is derived from the QLVM frequency (28 meV) (see Table 9.5.8). The charge state is proposed in a comparison with the other $\mathbf{V}_1\mathbf{Ni}_2$ centers, i.e., the $^*\mathbf{V}_1\mathbf{Ni}_2^+$ center (6) at 1.693, 1.940, and 1.991 eV, and the $^*\mathbf{V}_1\mathbf{Ni}_2^-$ center (10) at 2.071 and 2.298 eV. There is a general trend for decreasing charge state with increasing energy.
5. $^*(\mathbf{V}_2\mathbf{Ni}_1)\mathbf{N}_{x+y+z}^+ =^*$ Ni-S9-DAP4a-I (1.678–1.821 eV). This is a typical member of the S2 to $^*\text{S9}$ family (see Sect. 9.5.10 and Table 9.5.10). This center is absent in as-grown synthetic or natural diamonds, but appears after nitrogen implantation and 950°C annealing.
6. **(a-c)** $^*\mathbf{V}_1\mathbf{Ni}_2^+ =$ Ni 1.69a-c at (a) 1.693, (b) 1.940, and (c) 1.991 eV. Broad peaks are observed in absorption from (a) at 1.85 eV and from (b,c) at 2.16 eV. In luminescence, the broad peak is at 1.85 eV from (b,c)-DAP11a-f (1.708–1.898 eV). The expected resolved DAP transitions from the other lines are not yet observed. For the charge state, see line (4) at 1.660 eV.
7. **(a,b)** $^*\mathbf{V}_1\mathbf{Ni}_1^\circ =$ Ni 1.70a,b at (a) 1.704 and (b) 2.401 eV. Line (a) with DAP83a-f (1.816–2.070 eV) in absorption, and with DAP84a-c (1.568–1.627 eV) in luminescence. Line (b) with DAP29a-f (2.713–2.965 eV) in absorption.
8. $^*(\mathbf{V}_2\mathbf{Ni}_1)\mathbf{N}_{x+y+z}^+ =^*$ Ni-S7-DAP11a-n (1.808–2.620 eV). The EPR counterpart is the paramagnetic $S = 1$ center [Iak00a]. The single nickel atom follows from the isotope shifts (see Table 7.5 and Sect. 9.5.2). For the number of nitrogen atoms in the first shell, see Sect. 9.5.2.9 and Table 9.5.6.
9. **(a-c)** $^*(\mathbf{V}_3\mathbf{Ni}_2)^\circ =^*$ Ni 1.88a-c at (a) 1.883, (b) 1.906, and (c) 1.913 eV. Line (a) with DAP107a-g (1.958–2.300 eV) in absorption, and DAP108a,b (1.779, 1.808 eV) in luminescence. The structure is derived from the similarity with the better established $^*(\mathbf{V}_3\mathbf{Si}_2)^\circ$ center at 1.681 eV (see Sect. 8.1.6 and Table 8.1.6). The involvement of Ni_2 is derived from the LVM frequency (61 meV) (see Table 9.5.7). The neutral charge state follows from Tables 10.4 and 10.5.
10. **(a, b)** $^*\mathbf{V}_1\mathbf{Ni}_2^- =^*$ Ni 2.07 at (8a) 2.071 and (b) 2.298 eV. Line (a) with DAP87a-n (1.709–1.962 eV) in luminescence. Line (b) with DAP27a-j (2.3909–2.568 eV) in absorption and DAP28a-I (1.905–2.089 eV) in luminescence. The involvement of Ni_2 follows from the QLVM frequency (30 meV) (see Table 9.5.8). For the charge state, see line (4) at 1.660 eV.
11. **Ni + X** $=^*$ Ni 2.16 at 2.157 eV. This center with an unknown structure is observed after nickel implantation and $1,440^\circ\text{C}$ annealing [Zai00a]. The QLVM frequency (40 meV) indicates a (1 Ni + 1 C) vibration (see Table 9.5.8).

12. $\text{Ni} + X =^* \text{Ni}$ 2.27 at 2.267 eV. For this center with an unknown structure, many references exist in the literature (see [Zai01]). The line is assigned to nickel because of the close relation to the established nickel centers **S2** and **S3**.
13. $^* \text{V}_1 \text{Ni}_3^\circ = \text{Ni}$ 2.37 at 2.370 eV (named “A” line) with DAP91a–g (2.460–2.641 eV) in absorption and DAP92a–f (2.170–2.280 eV) in luminescence. The involvement of Ni_3 is derived from the QLVM frequency (23 meV) (see Table 9.5.8). The neutral charge state follows from the dielectric factor D (1.34 eV), which is expected for 3Ni with 84 total electrons (see Table 10.4).
14. $(\text{V}_2 \text{Ni}_1) \text{N}_{2+0+0}^+ = \text{Ni-S3-DAP58a-i}$ (2.496–2.890 eV). The complex structure and charge state of this center are established, because the EPR counterpart NE1 has been carefully analyzed [Yel92a],b, [Nad93] (see Sects. 9.5.4 and 9.5.10).
15. $(\text{V}_2 \text{Ni}_1) \text{N}_{2+0+1}^+ = \text{Ni-S2-DAP57a-n}$ (2.515–3.341 eV). Similar to line (14) = S3, the structure is established by analysis of the EPR counterpart NE2.
16. $\text{Ni}_1^- = \text{Ni}$ 2.51 at 2.510 eV. The structure and charge state are derived from the EPR counterpart WE8 (see Sect. 9.5.4).
17. $(\mathbf{a-d}) \text{ } ^*(\text{V}_3 \text{Ni}_2)^+ = 2\text{Ni}$ 2.56 at (a) 2.562, (b) 2.588, (c) 3.065, and (d) 3.076 eV. Line (a) with DAP105a–d (2.780–3.221 eV) in absorption and DAP106a–f (2.383–2.466 eV) in luminescence. The incorporation of two equivalent nickel atoms is evident from the isotope line shifts (see Table 7.5 and Sect. 9.5.2). For the positive charge state, see line (9) and Table 10.5.
18. $^*(\text{V}_2 \text{Ni}_1) \text{N}_{x+y+z}^+ =^* \text{Ni-S6-DAP61a-m}$ (2.750–3.530 eV). This center is absent in as-grown synthetic or natural diamonds, but appears after heat treatment ($T > 2,200^\circ\text{C}$). The involvement of a single nickel atom follows from the QLVM frequency (42 meV) (see Table 9.5.8). For the positive charge state, see Sect. 10.5. A possible EPR counterpart is the NE8 center.
19. $(\text{V}_2 \text{Ni}_1) \text{N}_{1+2+0}^\circ = \text{Ni-}^* \text{S4-DAP59a-l}$ (3.333–3.820 eV). This center is sometimes named “NE3 center” after the EPR counterpart NE3, from which the structure is established. In this book, the name $^* \text{S4}$ is introduced. Note the different charge states: Positive (EPR) and neutral (optics).
20. $^*(\text{C}_2)_i \text{Ni}_1^\circ =^* \text{Ni}$ 2.44 at 2.436 eV with DAP14a–f (2.066–2.271 eV). The structure $^*(\text{C}_2)_i \text{Ni}_1^\circ$ is assigned to the 2.436 eV -DAP14 center (Table 9.5.1.2) with the following arguments: 1.) The sample of Fig. 7.90 in [Zai98] contains nickel (see the line at 2.427 eV from $^* \text{V}_1 \text{Ni}_2^\circ$ (b) = no. 4(b) above). 2.) The sample with the Ni2.44 eV center contains $(\text{C}_2)_i$ (see the line at 3.188 eV from $^*(\text{C}_2)_i \text{N}_1^-$). 3.) The dielectric factor ($D = -1.22$) is in the expected range for associates with $(\text{C}_2)_i$ (see Table 8.2.3). 4.) The $^* \text{Ni}2.44$ eV center anneals out at 1300°C , which is typical for associates with $(\text{C}_2)_i$ (see Sect. 8.3.1). 5.) The ZPL (2.436 eV) of the $^* \text{Ni}2.44$ -DAP14 lines coincides with a single line from the so-called 509 nm center (with unknown structure); however, the 509 nm center has quite different properties: It appears (as irradiated) after ion implantation, and is stable up to 1400°C , while the DAP14 lines disappear at 1300°C . This center is absent in as-grown synthetic or natural diamonds, but is created after carbon ion implantation and 1000°C annealing [Zai92a].

9.6 Cobalt in Diamond

In the synthesis of HTHP diamond, transition metals are normally employed as solvent catalysts. Nickel, cobalt, and iron are often used, occasionally also manganese or chromium. While nickel forms at least 18 optical centers in diamond (see Sect. 9.5), its direct neighbor in the periodic system behaves surprisingly differently.

The concentration of cobalt in HTHP diamond, which is grown from pure cobalt, is an order of magnitude less than the nickel concentration in comparable HTHP diamond, grown from a pure nickel melt. The first cobalt-related optical lines were reported in 1991 from HTHP diamond, grown from a pure cobalt melt at high temperature [Col91c], [Fie92]. As with the nickel centers, the cobalt centers are found only in the (1 1 1) growth sectors, which dominate in the high temperature-grown octahedral diamonds. With the present knowledge (see Table 9.6), six cobalt centers were observed: *Co1.47, *Co2.59, *Co2.89, *Co1.85, *Co-S5 with nine lines at 2.135–2.820 eV, and *Co 1.99. For three centers, a DAP analysis was possible: Standard *Co-S5 DAP104a–i, sideband *Co 1.85 DAP102a–f, and sideband *Co 1.99 DAP112a–f.

A very detailed study of cobalt-related centers appeared in 1996, including measurements on annealing effects (1, 500–1, 800 °C), radiative decay times (20 ns–159 μs), and temperature dependence (4–150 K) [Law96].

As shown in Table 9.6, all known cobalt lines can be assigned to six cobalt centers, which are all associates with one, two, or three lattice vacancies. Only one center (named *Co-S5, in analogy to the nickel *S5 center) contains nitrogen in addition.

After cobalt ion implantation and > 600 °C annealing, spectral lines from two cobalt centers (*Co-S5 and *Co2.59) were observed [Zai79a, Zai01].

9.6.1 The *Co 1.47 Center at 1.472 eV from $*V_1Co_1^+$

9.6.2 The *Co 2.59 Center at 2.590 eV from $*V_1Co_2^-$

The luminescence of this center is fast (decay time ca. 80 ns), and is more intense in cathodoluminescence than in photoluminescence. No detailed spectra is shown in [Law96]; therefore, no results on phonon sidebands or DAP transitions can be given. The corresponding lines of $*V_1Ni_2^-$ occur at 2.071 and 2.298 eV (see Table 8.3a).

9.6.3 The *Co 2.89 Center at 2.889 eV from $*V_1Co_2^\circ$

The luminescence of this center is fast. This center appears after annealing at $T > 1,500$ °C.

Table 9.6 Cobalt centers in diamond

Defect ^a	Observed	ZPL (eV)	DAP lines (eV)	DAP ^b	L (eV)	D (eV)	Name/comment
*V ₁ Co ₁ ⁺	HL	1.472	-	-	-	-	*Co 1.47/relatively broad (20 meV); in regions of low nitrogen concentration
*V ₁ Co ₂ ⁻	ML (1,500 °C) Co impl. (600 °C)	2.590	-	-	-	-	*Co 2.59/medium fast luminescence (ca. 80 ns)
*V ₁ Co ₂ ^o	ML (20 h, 1800 °C)	2.889	-	-	-	-	*Co 2.89/fast lum./appears after annealing at T > 1,500 °C
*V ₁ Co ₂ ⁺	MA (24h, 1600 °C)	1.852	1.992–2.187	SB 102a–f (weak)	ZPL	+1.30	*Co 1.85 a/very weak absorption/LVM: (4x) + 44 meV
*(V ₂ Co ₁) N _{1+x+y} ^o = *Co-S5	HL Co impl. ML	-	2.135–2.820	sta. 104a–i	1.948	+1.53	*Co-S5/slow lum. (109 μs)/additional lines from L' = 1.952, 1.960, and 1.966 eV (from exc. st. splitting of 4, 12, and 18 meV)/QLVM: –38; LVM: –100 meV
*(V ₃ Co ₂) ^o	HL (as-grown, anneals out at T > 1,500 °C)	1.989	1.772–1.914	SB 112a–f (weak)	ZPL	–1.37	*Co 1.99/fast lum. (< 20 ns)/additional lines at 1.984, 1.991 eV (the latter from 2 meV exc. st. spl.)/QLVM: (2x) – 25; LVM: –56 meV

^aN_{a+b+c} indicates the number of nitrogen atoms in the first (a), second (b), or third shell (c)

^bStandard DAP104 and sideband DAPs 102 and 112 with L = limiting energy and D = dielectric factor

9.6.4 The *Co 1.85 Center at 1.852 eV from $*V_1Co_2^+$

This center appears after annealing at $T > 1,500^\circ\text{C}$. Simultaneously, the *Co 1.99 (V_3Co_2) $^\circ$ center anneals out, probably by trapping two carbon interstitials, which are created during V_1N_3 (N3 center) formation, and start to migrate at this temperature (see Sect. 9.1.6.1).

The 1.852 line is not yet observed in luminescence (1.693 eV luminescence for $V_1Ni_2^+$ (a), see Table 8.1.4), but the *Co 2.89 line of $*V_1Co_2^\circ$ is clearly present in the luminescence spectrum with 0 μs delay, together with the V_1N_3 (N3 center) line at 2.985 eV.

9.6.5 The *Co-S5 Center in the Range 2.135–2.820 eV from $*(V_2Co_1)N_{x+y+z}^\circ$

The spectroscopic lines of this center (luminescence only for the cobalt center, but both luminescence and absorption for the nickel *S5 center) arise from the standard DAP104a–h transitions. There is no ZPL, and the relative intensities are sample dependent, with intense lines at **2.135** eV ($s = 50$), **2.207** ($s = 26$), **2.277** ($s = 16$), and **2.367** ($s = 10$), and weak lines at 2.244 eV ($s = 26$), 2.330 ($s = 12$), 2.682 ($s = 3$), and 2.820 ($s = 1$). The radiative decay time for the slow luminescence has been determined for four lines [Law96]: 63 μs for $s = 10$ (donor–acceptor separation = 6.3 r_0), 109 μs for $s = 16$ (8.0 r_0), 159 μs for $s = 26$ (10.2 r_0), and 235 μs for $s = 50$ (14.1 r_0). The decay time increases approximately with the square of the distance, and this is a direct confirmation for the DAP interpretation of the *Co-S5 lines.

The dielectric factor of +1.53 eV indicates association with a single nitrogen in the first shell (in analogy to the $*(V_2Ni_1)N_{x+y+z}^\circ = *S5$ center in the range 1.563–2.320 eV and $D = +1.53$ eV, see Table 8.3b). The weaker sidebands with separation of 4, 12, and 18 meV arise from DAP transitions with a slightly higher limiting energy L' : 1.952, 1.960, and 1.966 eV. The temperature dependence indicates a corresponding splitting in the excited state. Like in Sect. 9.6.3, an alternate interpretation is a possible depopulation by energy transfer between slightly inequivalent centers.

9.6.6 The *Co 1.99 Center at 1.989 eV from $*(V_3Co_2)^+$

The $*(V_3Co_2)^\circ$ center is observed in as-grown samples, and anneals out at $T > 1,500^\circ\text{C}$. The ZPL is split into three components (1.9835, 1.9886, and 1.9906 eV). The difference (2 meV) between the latter two lines is ascribed to an excited state splitting. However, the Boltzmann analysis yields besides the correct activation

energy (2.47 meV) an additive constant of 0.29 to the ratio of the intensities. Therefore, an alternate interpretation is a possible depopulation by energy transfer between slightly inequivalent centers.

The corresponding $^*(V_3Ni_2)^+$ center has three lines at 1.883, 1.905, and 1.913 eV (see Table 8.1.6).

9.6.7 Discussion of Spectral Data from Cobalt Centers in Diamond

Cobalt has only one stable isotope of mass 59, and no frequency shifts from other isotopes can occur. Possibly, a paramagnetic center from cobalt has been observed [Col00].

In comparison with the corresponding nickel centers, the cobalt lines have the following:

Higher ZPL (10%) energies for *Co 1.85 and *Co 1.99 (*Ni 1.69 a and *Ni 1.88 a).

Higher ZPL (20%) energies for *Co 2.59 (*Ni 2.07 a).

Higher L (30%) (limiting energy) for $^*Co-S5$ ($L = 1.948$) ($^*Ni-S5$, $L = 1.460$ eV).

In contrast to the nickel centers, the influence of the nitrogen concentration on the cobalt lines is unspecific. In samples with low nitrogen concentration and in samples with 90% Fe dilution (10% Co), most Co lines are absent or very weak.

The LVM and QLVM frequencies are very similar for cobalt and nickel centers (see Tables 11.1 and 11.2).

The observed LVM frequencies are as follows:

(4x) + 44 meV for $^*(V_1Co_2)^\circ(a)$ from $Co(sp_3)-C(sp_3)$ bend.

(2x) - 60 meV for $^*(V_3Co_2)^+$ from $Co(sp_3)-C(sp_3)$ stretch.

(1x) ca. -100 meV for $^*(V_2Co_1)N_{1+x+y}^\circ$ from $Co-C/N(sp_3)$ stretch.

QLVM frequencies are observed at

(2x) - 24 meV for $^*(V_3Co_2)^+$ from $2Co + 4C$ (calculated 24.1 meV).

(1x) - 44 meV for $^*(V_2Co_1)N_{1+x+y}^\circ$ from $1Co$ (calculated 43.6 meV).

In theoretical cluster calculations on the transition metals V, Mn, Fe, Co, Ni, and Cu, their solubility in diamond and their long-range elastic strain have been investigated [Joh02]. Solvation enthalpy calculations for the impurity sites “substitutional,” “interstitial (no vacancy),” and “interstitial with divacancy” lead to the conclusion that nickel is the most likely transition metal impurity in diamond, and cobalt and copper following next. The lighter metals V, Mn, and Fe have unfavorable conditions for incorporation into diamond. These preliminary calculations are in good agreement with the experimental findings [Joh02].

9.7 Other Impurities in Diamond

Optical centers from 25 impurities (plus purely intrinsic centers from lattice vacancies or carbon interstitials) are observed in diamond. Only six impurities (H (see Sect. 9.3), B (see Sect. 9.2), N (see Sect. 9.1), Si (see Sect. 9.4), Ni (see Sect. 9.5), and Al (see NA2530 and NL2693a–e)) are found in natural diamond. The remaining 19 impurities are introduced by doping or ion implantation.

The 25 impurities can be divided into 15 main group impurities (Sect. 9.7.1 and Table 9.7.1) and ten transition metal impurities (Sect. 9.7.2 and Table 9.7.2). Six important impurities in diamond were treated in the preceding sections (Sects. 9.1–9.6). For 19 other impurities, optical centers are observed in diamond. Within Tables 9.7.1 and 9.7.2, the impurities are listed according to the main groups 1–8A and the transition metal groups 1–8B.

9.7.1 Main Group Impurities: H, Li, B, Al, In, Tl, Si, N, P, As, Sb, O, He, Ne, and Xe in Diamond

Out of the 36 main group elements, 15 impurities form optical centers in diamond (see Table 9.7.1). From group 1A, the light elements hydrogen (see Sect. 9.3) and lithium (also with bound excitons, see Sect. 9.7.6) are observed. Elements from group 2A are totally missing. From group 3A, the light elements boron (direct neighbor of carbon, see Sect. 9.2) and aluminum, together with the heavy elements indium (doping) and thallium (implanted), are optically active. For group 4A, only the light impurity silicon (see Sect. 9.4) is observed. In group 5A, the important nitrogen (direct neighbor of carbon, see Sect. 9.1), the light element phosphorous, and the medium heavy elements arsenic (doping) and antimony (implanted) give rise to optical centers. Only the light element oxygen (doping) from group 6A is optically active. Finally, the noble gas elements from group 8A, helium, neon, and xenon (all implanted), give rise to numerous lines.

9.7.2 Transition Metal Impurities: Ag, Zn, Ti, Zr, Ta, Cr, W, Fe, Co, and Ni in Diamond

Neglecting the lanthanides (element nos. 58–71) and actinides (nos. 90–103), there are ten elements (out of 30) in groups 1B–8B (see Table 9.7.2) with optical centers in diamond. From group 1B, *silver* (implanted) is observed. From theory [Joh02], copper (group 1B) is expected to be a stable impurity in diamond. In group 2B, *zinc* (implanted) is observed. No elements are found from group 3B. The two elements *titanium* (implanted) and *zirconium* (doping in the melt) are observed from group 4B. From group 5B, the heavy element *tantalum* (from hot filament

Table 9.7.1 Optical centers from main group impurities in diamond

Atom	Main group	Element no. = Z	Radius (nm) ^a	Electron configuration ^b	Observed lines and parameters (eV) ^{c-e}	Comment	Defect
H	1 A	1	(140)	1s ¹		11 centers, see Sect. 9.3 , DAP39, 40	
Li	1 A	3	77	He + 2s ¹		(Lum)*1.407-1.881 = SB-DAP68a-g, $D = -1.58$; (Lum) BE: 4.757-5.280	*V _i Li _i
B	3 A	5	(86)	He + 2s ² 2p ¹		16 centers, see Sect. 9.2 ; DAP1, 2, 17-20, 67, 70, 73, 74, 97, 99-101, (Lum) BE: 4.755-5.367	
Al	3 A	13	141	Ne + 3s ² 3p ¹		(A) 2.530, (Lum)*2.693-2.974 = SB-DAP66a-e, $D = -1.52$, (A,B) 2.990	*V _i Al _i
In	3 A	49	144	Kr + 4d ¹⁰ 5s ² 5p ¹		(A) 1.722	*V _i In _i ^{o?}
Tl	3 A	81	199	Xe + 4f ¹⁴ 5d ¹⁰ 6s ² 6p ¹		(Lum)*1.682-2.019 = SB-DAP94a-f, $D = -1.29$; implanted + HT	*V _i Tl _i ^o
C	4 A	6	76	He + 2s ² 2p ²		9 impurity-free centers (vacancies, interstitials), see Chap. 8.	
Si	4 A	14	119	Ne + 3s ² 3p ²		5 centers, see Sect. 9.4 , DAP8, 53, 54, 65, 75, 109, 110, and 113	
N	5 A	7	70	He + 2s ² 2p ³		42 centers, see Sect. 9.1 , DAP1, 4, 9, 18-20, 45, 67	
P	5 A	15	(110)	Ne + 3s ² 3p ³		(Lum, B) 1.900, (Lum, B) 2.066, (A) 2.637, (Lu,B) 4.450, (Lum)*4.711-5.275 = sta.-DAP2a-w, $D = +1.72$; $L = 4.500$; (Lum) BE: 5.020-5.333	P _i ^o + B _i ^o ,
As	5 A	33	120	Ar + 3d ¹⁰ 4s ² 4p ³		(A) 0.113-0.578 = SB-DAP115a-f, $D = +1.32$, * PC threshold = 0.524eV	*V _i As _i ^o

Sb	5 A	51	134	Kr + 4d ¹⁰ 5s ² 5p ³	(Lum) 2.705	
O	6 A	8	60	He + 2s ² 2p ⁴	(Lum) 2.676–2.725 = sta.-DAP17a–f, <i>D</i> = +1.29	*O ₁ ^o + B ₁ ^o
He	8 A	2	(90)	1s ²	(Lum)*2.049–2.212 = SB-DAP95a–f, <i>D</i> = –1.57, (Lum) 2.317, (Lum) 2.415	*V ₁ He ₁
Ne	8 A	10	150	He + 2s ² 2p ⁶	(Lum) 1.723, (Lum) 1.731, (Lum) 1.881, (Lum) 1.884, (Lum.) 2.393	*(V ₂ Ne ₁) ^o ?
Xe	8 A	54	233	Kr + 4d ¹⁰ 5s ² 5p ⁶	(Lum) * 1.235–1.528 = SB-DAP42a–j, <i>D</i> = –1.33	*(V ₂ Xe ₁) ^o

^a[Fin56], Fig. 1, with (interpolated) values

^b[Fin56], Table 11, complete shells: He = 1s²; Ne = He + 2p⁶, Ar = Ne + 3s²3p⁶, Kr = Ar + 3d¹⁰4s²4p⁶, Xe = Kr + 4d¹⁰5s²5p⁶

^cObserved: (A) = absorption, (Lum) = luminescence, (B) = broad, BE = bound exciton

^dDAP: sta. = standard, SB = sideband, *D* = dielectric factor, *L* = limiting energy, underlined = ZPL

^eQuasi-local vibrational modes (QLVM), see Table 8.7

Table 9.7.2 Optical centers from transition metal (TM) impurities in diamond

Atom	TM group	Element no. = Z	Radius (nm) ^a	Electron configuration ^b	Observed lines and parameters ^{c,d} (eV)	Name/defect
Ag	1 B	47	144	Kr + 4d ¹⁰ 5s ¹	(Lum) 2.842–3.111 = SB-DAP85a–f, D = –1.31, line (b) at 3.117	* (V ₂ Ag ₁) ^o
Zn	2 B	30	134	Ar + 3d ¹⁰ 4s ²	(Lum) 2.117–2.394 = SB-DAP114a–f, D = –1.42	* (V ₂ Zn ₁) ^o
Ti	4 B	22	150	Ar + 3d ² 4s ²	(Lum) 1.249, (Lum) 1.277, (Lum) 2.017, (Lum) 2.507	* (V ₂ Ti ₁) ^o
Zr	4 B	40	163	Kr + 4d ² 5s ²	(Lum) 1.443–1.565 = sta.-DAP5a–j, D = +1.39, L = 1.364	* (V ₂ Zr ₁) ^o
Ta	5 B	73	141	Xe + 4f ¹⁴ 5d ³ 6s ²	(Lum) 1.774–1.817 = sta.-DAP7a–e, D = +1.30, L = 1.685	* (V ₂ Ta ₁) ^o
Cr	6 B	24	126	Ar + 3d ⁵ 4s ¹	(Lum) 1.672, (Lum, B) 2.360	* V ₁ Cr ₁ ^o
W	6 B	74	138	Xe + 4f ¹⁴ 5d ⁴ 6s ²	(Lum) 1.723–1.759 = sta. (res.-)DAP6a–f, D = +1.24, LE = 1.608 (Lum) 2.557	* (V ₂ W ₁) ^o
Fe	8 (B)	26	129	Ar + 3d ⁶ 4s ²		

Co	8 (B)	27	128	Ar + 3d ⁷ 4s ²	6 centers, see Sect. 9.6, SB-DAP102a-f, $D =$ +1.30, ZPL = 1.852	*Co 1.85 =*
					sta.-DAP104a-h, $D = +1.53$, $L = 1.948$	V ₁ Co ₂ ⁺ *Co-S5 =* (V ₂ Co ₁) Ni _{1+x+y} ^o *Co 1.99 =* (V ₃ Co ₂) ^o *Ni 1.70a =* V ₁ Ni ₁ ^o
Ni	8 (B)	28	127	Ar + 3d ⁸ 4s ²	SB-DAP112a-f, $D =$ -1.37, ZPL = 1.989	*Ni-S5 =*
					18 centers, see Sect. 9.5, SB-DAP83/84, $D =$ ± 1.34 , ZPL = 1.704	(V ₂ Ni ₁) Ni _{1+x+y} ^o *Ni 1.88 =* (V ₃ Ni ₂) ^o
					sta.-DAP60a-g, $D = +1.53$, $L = 1.460$	
					SB-DAP107/108, $D =$ ± 1.34 , ZPL = 1.883	

^a[Fin56], Fig. 1

^b[Fin56], Table 11, complete shells: Ar = Ne + 3s²3p⁶, Kr = Ar + 3d¹⁰4s²4p⁶, Xe = Kr + 4d¹⁰5s²5p⁶

^cObserved: (A) = absorption, (Lum) = luminescence, (B) = broad

^dDAP: sta. = standard, res. = resonance, SB = sideband, D = dielectric factor, L = limiting energy

CVD deposition) is found. In group 6B, the elements *chromium* (implanted) and *tungsten* (from hot filament CVD deposition) are observed. No elements are found from group 7B. The light elements of group 8B are important for the catalytic melt of HPHT synthesis, and all three (with probability $\text{Ni} > \text{Co} > \text{Fe}$ [Joh02]) are incorporated in diamond. Optical lines from *iron*, *cobalt* (see Sect. 9.6), and *nickel* (see Sect. 9.5) are observed. For many of the 18 Ni centers, the HPHT melt is not the only source of nickel, because these centers are also found in natural or ion-implanted diamond.

9.7.3 *Effects of Annealing*

After ion implantation, annealing at $T > 1,000^\circ\text{C}$ is usually necessary. The interesting annealing effects of Ni centers are listed in Table 9.5.6.

9.7.4 *Local Vibrational Modes*

The observed LVM frequencies of H, B, N, Tl, Si, Ag, and Ni are discussed in Sect. 11.1.

9.7.5 *Quasi-Local Vibrational Modes*

The QLVM frequencies and line widths are discussed in Sect. 11.2. In Table 11.2 observed QLVM data are compared with calculated values. The agreement is very good.

9.7.6 *DAP Transitions*

For most of the 26 impurities, resolved DAP transitions are observed (see Tables 9.7.1 and 9.7.2). More DAP discussion is given in Sect. 9.7.7.

9.7.7 *Bound Excitons from Li, B and P*

In diamond, bound exciton lines from Li, B, and P are observed (see Table 9.2.6). In the literature, the boron [Ste97a] and phosphorous [Ste99a] bound excitons have been discussed.

9.7.8 Considerations for Structure Assignments

In columns 4 and 5 of Tables 9.7.1 and 9.7.2, the atomic radius and the electron configuration are given. The impurity X can form an associate V_1X_1 with the single vacancy, or (V_2Y_1) with the double vacancy (Y in an interstitial position). The atomic radius is an important hint for the stable configuration. Interestingly, Co and Ni with $r = 127\text{--}128$ nm occur in both configurations. The large Xe ($r = 233$ nm) requires the double vacancy. The configuration assignment is further supported by the QLVM frequency, which includes C_3 for V_1X_1 and C_8 for (V_2Y_1) (see Table 11.2).

The electron configuration is related to the type of DAP transitions (see Chap. 10). If the impurity in the double vacancy has a *partly* filled 3d, 4d, or 5d shell (like for Zr, Ta, W, Co, and Ni), the DAP transitions are of the *standard* type. In the case of a complete 3d or 4d shell (Ag, Zn, and Xe), the DAP transitions are of the *sideband* type. For the V_1X_n configurations ($n = 1, 2, 3, 4$), the DAP transitions are always of the *sideband* type.